The United Nations University

GEOTHERMAL TRAINING PROGRAMME
Orkustofnun, Grensásvegur 9,
IS-108 Reykjavík, Iceland

Reports 2006
Number 16

RESERVOIR EVALUATION OF THE ÖLKELDUHÁLS GEOTHERMAL FIELD, HENGILL AREA, SW-ICELAND

Joseph Patrick Odong Okedi
Ministry of Energy and Mineral Development
P.O. Box 7270, Kampala
UGANDA
jpokedi@gmail.com

ABSTRACT

In order to produce viably from a given geothermal reservoir, one needs to know its deliverability, properties and size. The Ölkelduháls geothermal field is one of at least seven geothermal fields in the Hengill high-temperature area in SW-Iceland located about 35 km east of Reykjavík, just north of the town of Hveragerdi. This field belongs to Orkuveita Reykjavíkur (Reykjavik Energy).

Warm-up and injection transient test and temperature and pressure profiles from well HE-20, exploration well ÖJ-1 and the recently drilled well HE-22 were used for estimating reservoir parameters, determining deliverability and establishing some of the reservoir's natural state concepts for a model. In HE-20, the pressure control point was manifested at about 1500 m depth, near the main feedzones which are located at about 1400 and 1600 m depth. Estimates of formation temperatures and initial reservoir pressures at these depths were obtained using the Horner method and the program PREDYP and found to be about 250°C and 85 bar-g, respectively. Using non-linear regression, the derivative plot, Theis solution, multiple rate techniques and type curve matching, fall-off and injection step test data were used to infer the permeability-thickness (*kh*) in the range from 9 to 84 Dm, storativity about 3×10^{-8} m/Pa.s, whereas skin was deduced between 0 and -3. The limits of the reservoir could not be determined and analyses could not establish whether the boundaries were open or closed. However, the radius of investigation for the period of the tests was evaluated as 3.6 km. Previous resistivity surveys approximate the reservoir at 20 km^2 in area. The deliverability of well HE-20 was determined by the Russell James critical lip pressure method and through simulation using the HOLA wellbore simulator. For the period of discharge, with a reservoir pressure of around 85 bar-a at the main feed, enthalpy was determined as 1115 kJ/kg at the wellhead. A maximum wellhead pressure of 16 bar-a and a productivity index of 9.1 kg/s/bar were estimated.

1. INTRODUCTION

The Government of Uganda (GoU) through the Ministry of Energy and Mineral Development is exploring options for the utilization of alternative sustainable energy resources to feed the increasing demand for electrical energy in the country. Feasibility studies of mini-hydro, geothermal, solar, peat,

wind, and biomass alternatives favour the development of geothermal energy as a relatively clean source of energy, with minimal environmental impacts that are largely predictable. Since energy development and environmental damage are intricately related, the main policy goal in the energy sector is "to meet the energy needs of Uganda's population for social and economic development in an environmentally sustainable manner". The government's energy policy recognizes the need to mitigate both the physical and socio-environmental impacts created by energy development.

Western Uganda lies in the western arm of the East African Rift System referred to as the Albertine Rift which has an estimated geothermal potential (electric) of 450 MW (McNitt, 1982). Various methods have been used in exploration including isotope hydrology, geological, geochemical and geophysical surveys. In the Kibiro and Katwe prospects, all these methods were consistent in establishing geothermal anomalies, subsequently leading to the siting of gradient wells which are being drilled to provide a basis for detailed structural mapping, resistivity surveys and structural geophysical surveys in the hope of:

a) Developing a structural model of the reservoirs;
b) Ascertaining drilling properties of the formation;
c) Determining temperature, pressure, and chemistry of potential aquifers;
d) Establishing the casing programme for deep wells;
e) Obtaining reliable data about the hydrothermal alteration, cap rock - indicating porosity and permeability; and
f) To approximate the boundaries of the reservoirs - thus estimating their potential.

With the above background, the Government of Uganda and International Development Partners are building the capacity to meet the above objectives. This report is part of a six month training course at the United Nations University Geothermal Training Programme in Iceland where the author presents findings and analyses of well test data from the Ölkelduháls field in the Hengill high-temperature geothermal area in SW-Iceland in order to estimate reservoir parameters. This field belongs to Orkuveita Reykjavíkur (Reykjavik Energy). Ölkelduháls is located in the Hengill volcanic massif about 35 km east of Reykjavík, just north of the town of Hveragerdi. The data is by courtesy of Orkustofnun and ISOR database, and Reykjavik Energy.

2. GEOLOGICAL BACKGROUND

2.1 Tectonic and geological settings

Hengill area is located in SW-Iceland within the western branch of the active volcanic zone (Saemundsson, 1979). It is one of the largest geothermal areas in Iceland, covering about 100 km^2. Three volcanic systems are found in the Hengill area. Graendalur volcano in the eastern part is extinct and deeply eroded. The others, Hengill and Hrómundartindur, are still active. The most recent eruptions in the Ölkelduháls area were at the end of the last glaciation some 10 thousand years ago. Each volcanic system is intersected by a fissure swarm which has the structure of a nested graben. The geological formations in the Ölkelduháls area (Figure 1) consist primarily of basaltic hyaloclastites and lavas related to the Upper Pleistocene and Postglacial series. The majority of faults, fissures, and hyaloclastite ridges strike NE-SW (Saemundsson et al., 1990). Fumaroles (steam vents) and hot springs in the Hengill area are distributed along the faults and fissures. An altered rock zone from Nesjavellir in the north across the eastern part of the Hengill volcano through Ölkelduháls to Hveragerdi in the south is formed due to the interaction between geothermal fluids and rocks surrounding the surface geothermal manifestation.

The hydrology of the Hengill area is of two types. In the western part, stable springs and streams formed only where the geological formations were so altered that they became impermeable.

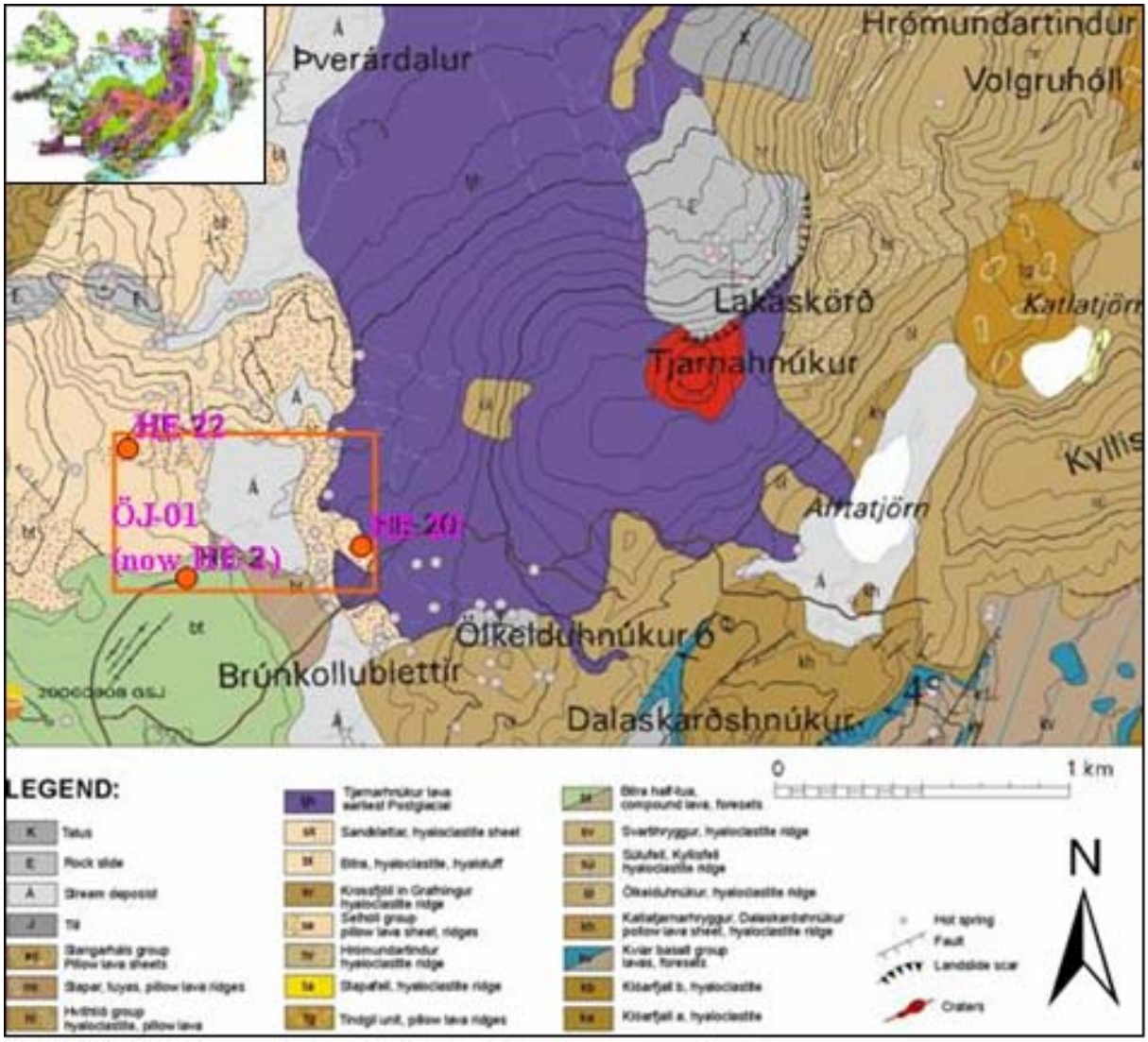

FIGURE 1: Hrómundartindur volcanic system showing the location of wells ÖJ-1, HE-20, and HE-22 in the Ölkelduháls geothermal field (modified from Saemundsson, 1995)

Otherwise, all water infiltrates down into the ground. In the eastern part of the area, rivers and streams flow all year round.

The Hengill complex is divided into at least seven geothermal fields: Nesjavellir, Hellisheidi, Hengladalir, Hverahlíd, Ölkelduháls, Graendalur (Grensdalur) and Hveragerdi. Reykjavik Energy operates geothermal power plants at Nesjavellir and Hellisheidi.

2.2 Ölkelduháls geothermal field

Tectonic features control geothermal activity in the Ölkelduháls high-temperature area. There is a marked NW-SE trend in the geothermal manifestations from Klambragil gully to well HE-20, probably controlled by a regional transform fault zone. However, most of the local manifestations are oriented in the general NE-SW trend of the faults and fractures in the Ölkelduháls area.

The feeder dykes of Molddalahnúkar appear to have created several fractures in Ölkelduhnúkur hill, enhancing the upflow of hydrothermal fluids and the occurrence of numerous manifestations. Most of the springs are carbonated and precipitate calcite and aragonite, an indication of vanishing geothermal

activity. Extinct clay alterations and mineral scaling reduce the permeability of the bedrock which has caused subsequent extinction of geothermal activity in some localities. (Natukunda, 2005)

2.3 Geophysical settings

Exploration of the Hengill area has extended over several decades with special attention to the Nesjavellir area in the eighties (Björnsson et al., 1986; Gunnarsson et al., 1992). However, in 1992 a central loop transient electromagnetic (TEM) survey was carried out and the results, which were encouraging. increased interest in the Ölkelduháls field. The resistivity survey conducted over the Hengill area shows a low-resistivity anomaly associated with the geothermal area (Figure 2). It is assumed to be related to a highly conductive layer (<5 Ωm) covering an area of about 100 km^2 which is interpreted as being caused by alteration and high porosity of rocks. Below the low resistivity, higher resistivity (>50 Ωm) is seen. Nearly all surface geothermal manifestations in the Hengill area are within the boundaries of the low-resistivity anomaly at sea level (Björnsson et al., 1986; Azimudin, 1995). The resistivity distribution is generally divided into three layers: an upper layer of high resistivity (>50 Ωm), a middle layer of very low resistivity (<10 Ωm) and a lower layer of high resistivity (>20 Ωm).

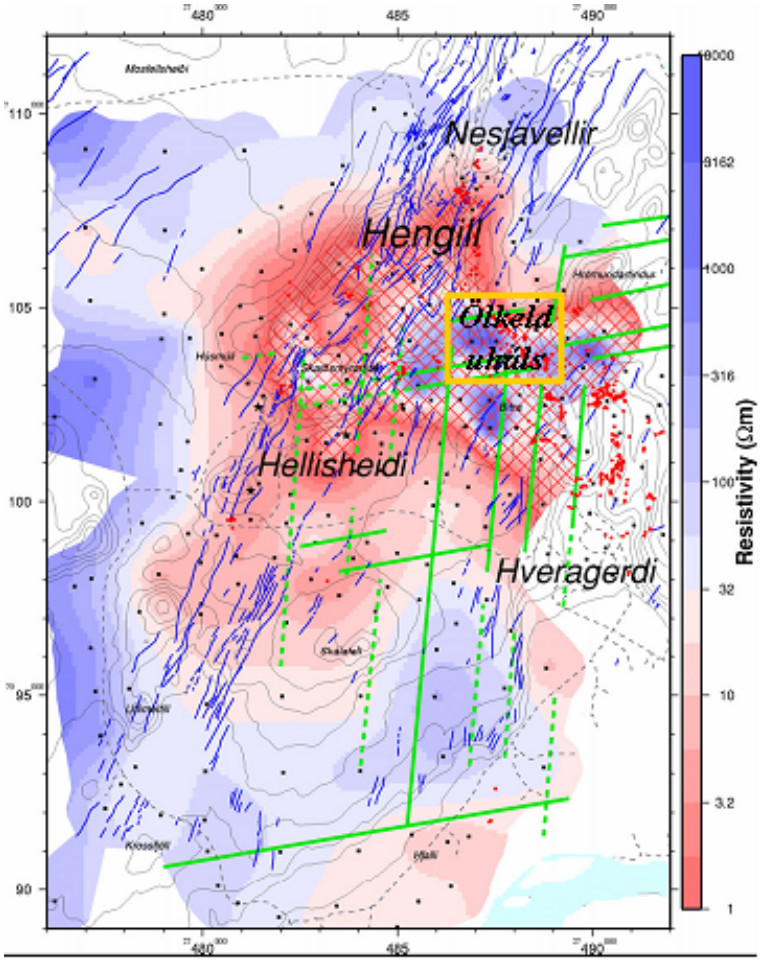

FIGURE 2: Resistivity at 100 m b.s.l. according to a TEM survey; also shown (in blue) are visible fault lines and (in green) faults as defined by earthquake locations; the rectangle shows the location of the Ölkelduháls geothermal field in the Hengill system (modified from Árnason and Magnússon, 2001)

The results of the TEM soundings were compared with those of Schlumberger soundings giving similar results, but demonstrating the better resolution and accuracy of the TEM data. One deep exploration well (ÖJ-1) was completed in January 1995 to a depth of 1035 m where it recorded an unexpected temperature of only about 198°C. Several downhole geophysical measurements were conducted during and after drilling. Both TEM soundings and resistivity logs identified the top of the geothermal reservoir (the caprock) at 120 m. Porosity values obtained from geophysical log calculations and core analysis show good correlation (Azimudin, 1995).

TEM findings revealed an extensive low-resistivity layer delineating the geothermal system with a pronounced increase in resistivity below the low-resistivity layer. The increase was interpreted to reflect transition in dominant alteration minerals from clays formed at intermediate temperatures (smectite and mixed-layer clays) to the high-temperature chlorite and epidote (Árnason, 1993). Geochemical and resistivity studies indicate that Ölkelduháls and Nesjavellir

geothermal fields are not connected at depth and can, therefore, be exploited independently (Ívarsson, 1998). Ölkelduháls field has been designated for future development of both electricity production and hot water production for space heating. Gas geochemistry measurements predict a reservoir temperature of about 300°C.

3. WELL TESTING AND WELL TEST DATA

It is important to understand why well testing is essential. From a public sector perspective, governments are required to keep tabs on reserve size, revenue accounting, and to provide a level playing field for all companies. Generally, the objectives of a well test fall into three major categories namely: reservoir evaluation, management, and description. This project was intended to evaluate the geothermal reservoir at the Ölkelduháls field.

During a well test, the response of a reservoir to changing production (or injection) is monitored. Since the response is, to a greater or lesser degree, dependent upon the properties of the reservoir, it is possible to infer some of these properties from the response. Well test interpretation is therefore an inverse problem in that model parameters are inferred by analyzing the actual response to a given input.

Information typically obtained from pressure transient tests includes: effective permeability or permeability thickness, detection and magnitude of formation damage or stimulation surrounding the well, detection and approximate distances to flow barriers and fluid contacts and communication between wells.

3.1 The design of a well test

A well test is intended to meet specific reservoir analysis objectives. To meet the required objectives, a test must be properly designed. An improperly planned test results not only in fruitless expense, it also fails to provide the desired reservoir data. In some cases, it may not be possible to attain the required objectives at all, and in other cases special equipment may need to be ordered in advance and transported to the well site. For all these reasons, it is essential to carefully consider what the test is expected to achieve, and how it is to be performed to successfully reach those goals.

Effective well test design requires consideration of which operational variables affect the estimates of which reservoir variables. For the most part, the operational variables under the control of the engineer are the flowrate and the duration of the test. A choice must also be made as to the type of test to be carried out. There are various types of tests that can be carried out for purposes of parameter analysis and/or characterization including but not limited to:

- Drill stem testing (DST);
- Modular dynamics testing (MDT) / flowrate testing (FRT);
- Pressure build-up;
- Pressure drawdown;
- Multi flowrate;
- Fall-off;
- Injection;
- Step rate;
- Interference;
- Pulsed testing; and
- Repeat formation testing (RFT).

This section is divided into three parts: consideration of the effects of flowrate and time, specification of the test duration, and appraisal of the flowrate.

3.1.1 Variable dependency

Understanding which variables depend on which is of assistance in planning the test. In designing the operation, there are two major considerations; (a) will the reservoir parameter to be estimated affect the well pressure in a significant enough way that the effect will be detectable with the tools available to measure and analyze the response; and (b) will the test be of sufficient duration for the response of interest to be seen?

3.1.2 Test duration

The overall period of time for which the test must be conducted has to be sufficient to be assured of reaching the part of the reservoir response that is of interest. For example, if the objective of the test is to evaluate the effectiveness of an acidization treatment in removing skin damage, then it is necessary to obtain sufficient data past the end of the storage transition to be assured of recognizing the correct semi-log straight line.

3.1.3 Flowrate considerations

The pressure change is directly proportional to the flowrate in all but a few special cases. Thus, it is necessary to determine whether the maximum flowrate change attainable will provide sufficient pressure change over the part of the response curve most diagnostic of the reservoir parameters of interest. For example, a highly permeable reservoir may have only a very small pressure change during the semilog straight line period of its response. If this change is so small as to be adversely influenced by measurement noise, it will then be difficult to obtain good estimates of the permeability.

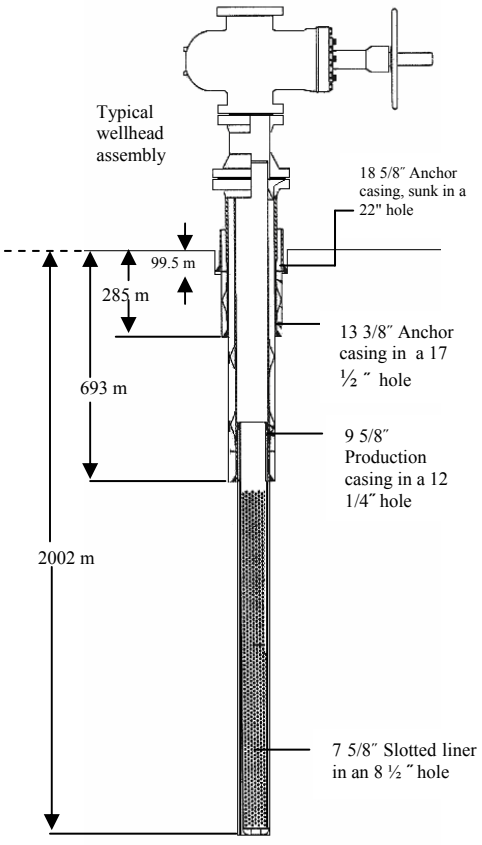

FIGURE 3: Casing programme for well HE-20; the well was unintentionally slightly deviated below the production casing (Mortensen et al., 2006)

3.2 Well test data from Ölkelduháls geothermal field

3.2.1 General information on wells

Well ÖJ-1 at Ölkelduháls is an exploration well drilled to a total depth of 1035 m during the period October 10, 1994 to January 22, 1995. Its UTM coordinates are shown in Appendix I (Table 1); the casing program used has an 18 ⅝" conductor casing to a depth of 79 m with a 21 ¼" flange pipe. The 13 ⅜" anchor casing is sunk to a depth of 301 m, while the 9 ⅝" production casing reaches 777 m depth. It was fitted with a 7 ⅝" slotted liner from 734 m depth to 1013 m (Steingrímsson et al., 1997). The permeability of this well is very high, especially at the bottom hole feed zone, with an estimated transmissivity of about 0.8×10^{-11} m^3/s bar (Azimudin, 1995).

Additional wells HE-20 (Figure 3) and HE-22, completed in December 2005 and July 2006 have since been drilled

to depths of 2002 and 2104 m, respectively. The UTM coordinates and the casing programs are also shown in Appendix I. The analyses of these wells are discussed in the proceeding sections.

3.2.2 Interpretation of temperature logs

In temperature logs during injection, a loss of fluid is seen as a slight change in the gradient of the temperature profiles, whereas fluid gain is reflected by a discontinuous jump in temperature (Stefánsson and Steingrímsson, 1990). Figure 4 shows multiple temperature logs from ÖJ-1. The earlier logs were done during drilling while water was being injected into the well. There are other temperature logs for the heating-up period after drilling. Annular measurements of the temperature in the well have been monitored since 1995. These logs are also shown in Figure 4. The dashed curve shows the estimated formation temperature based on measurements in the well.

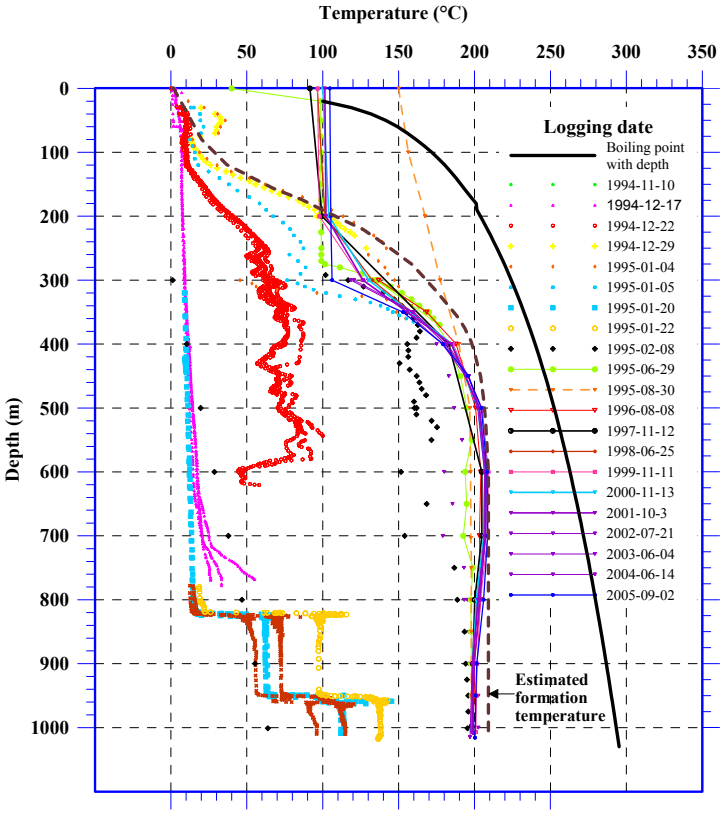

FIGURE 4: Plot showing the temperature profiles of well ÖJ-1 and the boiling point with depth curve

When there is no flow between aquifers, the temperature in the well will usually reach equilibrium with the surrounding rock. However, processes like boiling, accompanied by one-dimensional convection, can disturb the temperature profile in a well. All high-temperature wells tap reservoirs of greater temperatures than 200°C. Boiling and steam accumulation will, therefore, always be present in these wells during discharge at atmospheric pressure and sometimes even when they are closed.

The boiling point of water is defined by two parameters, temperature, and pressure. At atmospheric pressure water boils at the well known temperature of 100°C. If the pressure is high, a higher temperature is needed to reach the boiling point. It is common in temperature log interpretation to compare the temperature profiles measured in closed wells with a boiling point curve. Figures 4 and 5 show the boiling point with depth curve for water. This curve is derived by assuming that the water column in the well is at boiling point temperatures from the water level down to the bottom of the well. The comparisons immediately show where boiling can possibly occur in the well.

Well ÖJ-1: One of three wells analysed. As it is non-artesian, the well had to be stimulated to flow. The water level was at 300 m (Steingrímsson, pers. comm.) with a flow of about 30 kg/s at a 5 bar wellhead pressure (*Po*), at an elevation of 361 m a.s.l. Circulation losses, downhole temperature (Figure 4) and pressure profiles shortly after drilling suggest that there are three aquifer systems intercepted by the well, at 14 (8°C) and 68 m (34.4°C) depths indicating cold groundwaters, and finally a geothermal system from 400 m to the bottom. The well has three obvious feed zones from the geothermal system. During injection a fluid gain is seen as a discontinuous jump in the temperature profile. Such jumps at 820 and 960 m are a clear indication of feed zones. The injected fluid and the additions from the feed zones flow down the well and into a feed zone at the bottom.

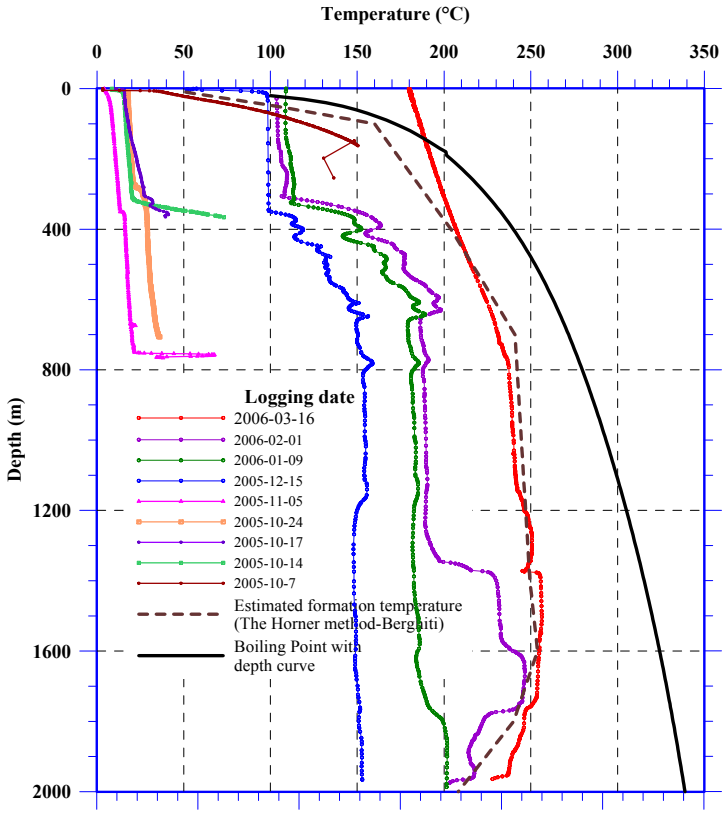

FIGURE 5: Plot showing the temperature profiles of well HE-20 and the boiling point with depth curve; arrows indicate direction of fluid flow

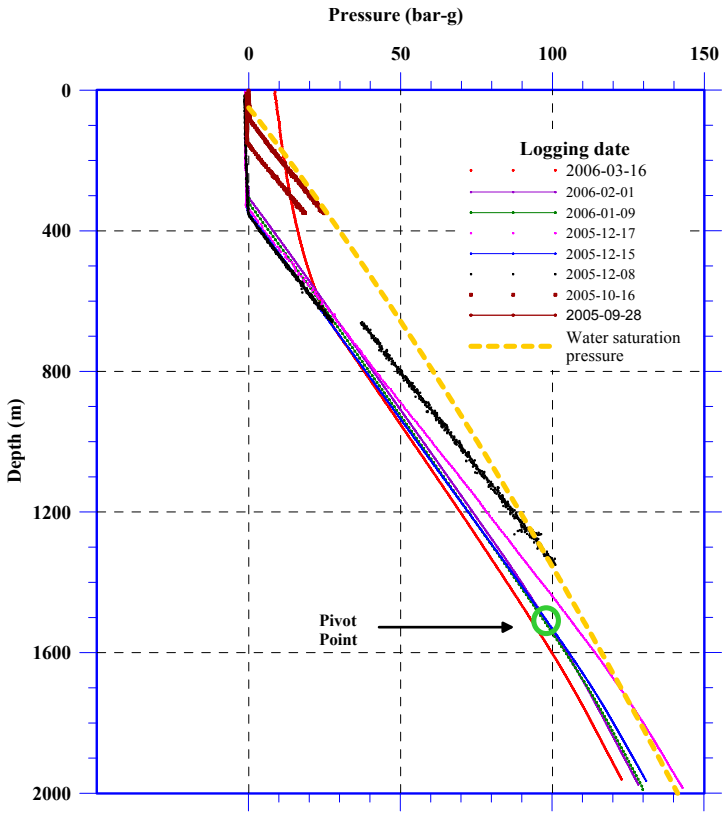

FIGURE 6: Plot showing pressure profiles for well HE-20 and the water saturation pressure profile

The temperature of the geothermal aquifer system is close to 200°C. However, the temperature above 400 m decreases gradually up to the surface and is typical of conductive heat transfer through the formation, implying that this curve could be closely representative of formation temperature.

Well HE-20 is at an elevation of 350 m a.s.l. During the flow test, it discharged 30-40 kg/s at 10-12 bar well head pressure (Po). Temperature and pressure profiles measured soon after drilling show a water table at about 350 m depth. The temperature logs (Figure 5) show the existence of several feed zones in the well. Feed zones above 700 m are cased off and, therefore, do not flow into the well but show up in the logs as "cold spots". The temperature logs in the production part below 700 m show an internal flow with shallow inflow down the well. The inflow can be seen in the logs at 700, 780, 1200, 1400 and 1600 m and the down flow disappears into a feed zone at 1800 m depth. The latest logs in HE-20 were done with the well discharging (dynamic logging). Both the temperature logs in Figure 5 and the pressure logs in Figure 6 show that the boiling level during discharge was at about 800 m depth. The maximum temperature measured in this well is 256.4°C at 1503 m depth (2006-03-16 log). The temperature data from well HE-20 has been analysed using Horner plots to estimate formation temperature (see Section 3.2.3). The result of the study is the dashed profile in Figure 5. It shows fairly isothermal temperatures of 240-255°C from 700 to 1600 m. Above 700 m, a conductive gradient is estimated, and below 1600 m an inversion is predicted. The temperature inversion starting at 1800 m depth means that the temperature decreases with depth, probably due to lateral flow in the reservoir. It should be remembered that all the temperature logs were done shortly after drilling and it is possible the temperature at the

bottom section of the well is still cooled after drilling. Temperature logs in the future will either confirm or reject the proposed temperature inversion below 1600 m in well HE-20.

Well HE-22 was completed in July 2006 and is still undergoing recovery after drilling was stopped. Its elevation is 374 m a.s.l. Temperature and pressure profiles soon after drilling suggest the presence of a feed zone at 1100 m depth. The highest temperature logged at the time of writing this report was only 119°C at 1708 m depth (2006-07-10). However, an initial discharge temperature of 200°C was recorded from the well on August 25, 2006.

3.2.3 Estimation of formation temperature

Formation temperatures serve as a pedestal for a conceptual model of a geothermal reservoir but are also important for making decisions upon well completion. However, due to cooling by circulation fluid during drilling, it is not possible to measure the formation temperature directly during drilling. Even if months or years have passed, boiling or convection may occur in the well, hiding the formation temperature.

The program BERGHITI in the ICEBOX program package (Arason et al., 2003) was used for analysis of post-drilling thermal recovery data of well HE-20 in order to estimate the formation temperature. The program uses the Albright and Horner methods to determine the estimates. The Albright method estimated higher temperatures than the measured dynamic profiles, probably indicative of the situation during formation.

The Horner plot method is, on the other hand, a simple analytical technique for analyzing maximum bottom-hole temperatures to determine the formation temperature. The basic criterion for the technique is the straight line relationship between the maximum bottom-hole temperature, T, and $\ln(\tau)$ with

$$\tau = \left(\frac{\Delta t}{\Delta t + t_0} \right);$$

where Δt = The time passed since circulation stopped;
t_0 = The circulating time; and
$\lim_{\Delta t \to \infty} \ln(\tau) = 0$.

After an infinite time, the system is assumed to have stabilised and it is then possible to determine formation temperature by plotting the maximum bottom-hole temperatures as a function of ln (τ) and drawing a straight line through the data where we obtain the ln (τ) intercept.

The estimate of formation temperature of HE-20 obtained using the Horner method is shown in Figure 7 and is also compared with temperature profiles obtained from logs in Figure 5. It is evident that as the well approaches thermal equilibrium, the warm-up temperature profiles get closer with time.

Nonetheless, the method is valid only for wells with no internal flow that are undergoing conductive warm-up.. Formation temperatures were estimated from temperature logs taken during and after drilling for well ÖJ-1 (see the dotted lines in Figure 4). Clearly, bottom-hole temperatures (BHT) were more representative of the formation temperature as there was less cooling at the bottom at the time of logging. The measurements were usually just shy of the actual values. When equilibrium was attained during warm-up, the last temperature log was assumed to represent the formation temperature. At a depth of 800 m, it was estimated that the formation temperature in the geothermal reservoir around well ÖJ-1 was about 210°C.

At the time of writing this report, only scanty data were available for well HE-22, thus the formation temperature could not be determined reliably.

3.2.4 Estimation of initial reservoir pressure

The pressure pivot or *pressure control point* concept is crucial to understanding well behaviour during the warm-up period. When a well is filled with liquid, the pressure gradient is controlled by the fluid density (hydrostatic). In the ideal case of a well with a single main feed zone, pressure in the well at the depth of this feed zone will be controlled by and will equal the formation pressure. Thus, as the wellbore fluid changes temperature during the heating period, the density of fluid also changes, but pressure at the feed zone is fixed by the formation pressure, so the pressure profile observed in the well pivots about the feed depth. For this type of well the pivot uniquely identifies this depth.

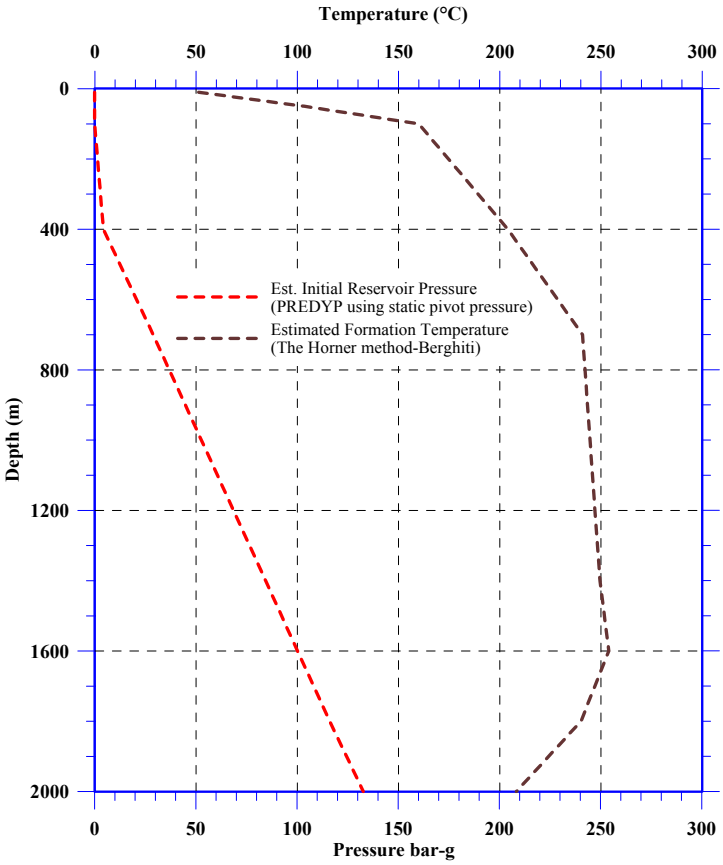

FIGURE 7: Plot showing estimated initial conditions of the reservoir in the proximity of well HE-20

When a well has multiple feed zones the pivot point will normally appear between the extremes of these, at a depth that is weighted by their productivities and injectivities. For these wells there will also be associated internal wellbore flow between zones resulting from the pressure differences (as opposed to the ideal single zone case, where there is no internal flow). Temperature and pressure profiles for well HE-20 indicate the main feed zones to be those at 1400 and 1600 m depth as shown by the location of the pressure pivot at 1500 m (Figure 6).

The location of the pivot point, relative to the feed zone depths, indicates the relative importance of the separate zones. That is, if the pivot is midway between the major zones, then they will have approximately equal productivity-injectivity, whereas if the pivot is very close to either the top or bottom zones, then that zone is dominant. In the multiple zone case, a major zone near the pivot may be hidden by the effects of other zones some distance above and below. Where other information is unavailable the depth and pressure at the pivot point are the best indicators of formation pressure for multiple-feed wells. The observed temperature-pressure conditions in the wellbore during warm-up then reflect internal flow, or static conditions that are the result of pressure differences between the wellbore and the formation.

TABLE 1: Initial reservoir conditions at HE-20

Depth (m)	Estimated reservoir pressure (bar-a)	Estimated formation temperature (°C)
10	-	51.2
50	-	103.4
100	-	160.0
400	4.3	204.0
700	28.9	240.9
1400	84.5	249.5
1600	100.3	253.9
1800	116.2	240.1
2000	132.8	208.2

The formation temperature was used to calculate the pressure at given depths in the formation

(Table 1). Before casing, the initial pressure profiles corresponded to the values obtained during drilling. However, after positioning the production casing, the pressure below this depth was estimated using the ICEBOX program PREDYP. The program was fed the formation temperature data and static pressure conditions at the pivot point (Arason et al., 2003). Through wellbore simulation of HE-20, the reservoir pressure was estimated to be 84.5 bar-a at 1400 m depth near the pressure pivot point. The pressure pivot for well ÖJ-1 is at a depth of about 680 m (Figure 8) which, according to the measured temperature profiles (Figure 4), is near one of the feed points located at a depth of about 820 m. The average pressure over this zone was about 36 bar-a.

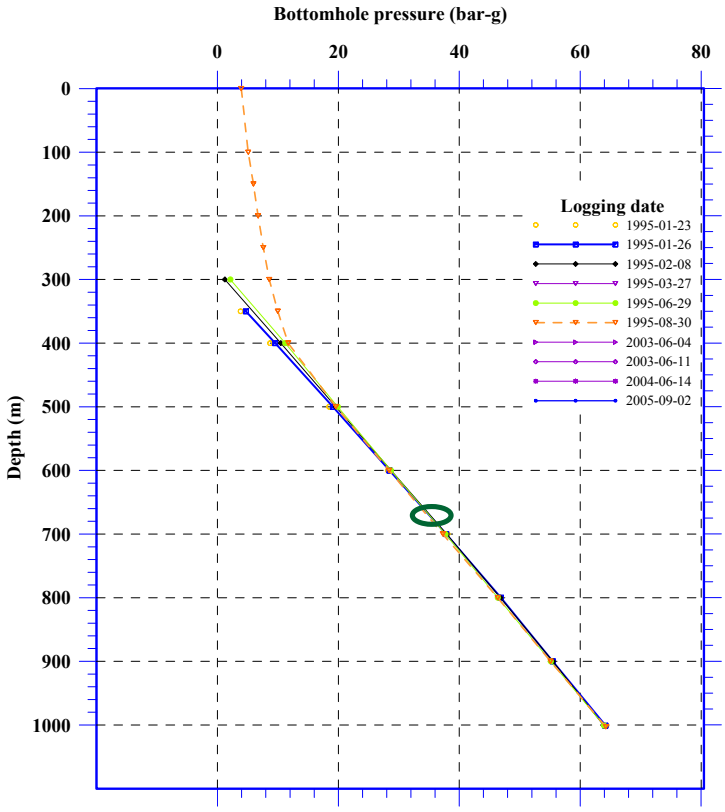

FIGURE 8: Plot showing pressure profiles with depth for well ÖJ-1

3.3 Conceptual models

3.3.1 Temperature and pressure distribution

Figure 9 shows the estimated initial reservoir temperature distribution in the Ölkelduháls field at 600 m depth below sea level. Figure 10 shows the pressure distribution at 600 m depth b.s.l. The direction of fluid flow is to the northeast, probably following the general NE-SW fault line orientation of the active volcanic zone in Iceland. However, according to reports of recent geothermal exploration activities in the area, there is a marked NW-SE trend in the geothermal manifestations from the Klambragil gully to well HE-20. There is also a general W - E trend of deep rooted seismic faults around the field, although most of the local manifestations are oriented in the general NE-SW trend (see Figure 2). The orientation of faults and fractures in the Ölkelduháls area may account for the colder fluid flow to the southeast (Figure 9) where it intercepts the general NE-SW trend and at the same time flows into a hotter zone and consequently heats up. Naturally the warmer fluid will seek out fissures in the faults and thus flow to the northeast, as shown in both Figures 9 and 10. Therefore, according to the temperature distribution shown, the siting of well HE-20 could not have been any better as it was drilled within the probable location of the heat source of the geothermal field.

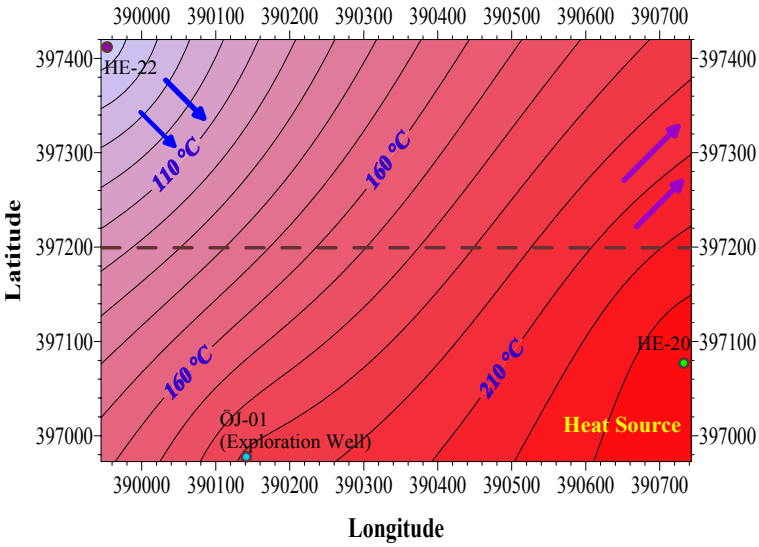

FIGURE 9: Temperature distribution (˚C) at 600 m b.s.l. in the Ölkelduháls field; the broken line is the line of a W-E cross-section through the field

3.3.2 Temperature cross-section through the field

Figure 11 shows a W-E temperature cross-section across the Ölkelduháls geothermal field. The hottest part of the reservoir seems to be penetrated by well HE-20. The recharge and regional flow through the NW-SE oriented fissures and fractures is likely to be responsible for the cooling tendency of the formation below 1600 m b.s.l. This is visible in Figures 7 and 11. These figures seem to indicate that well HE-20 penetrates the hottest parts of the reservoir. The general trend of fault lines is in a NE-SW direction which explains the preferred direction of fluid flow across the section. TEM soundings (Figure 2) show that the area of the field east of HE-20 has formation temperatures above 250°C and could easily qualify as the upflow zone of the reservoir. The cap rock is estimated by the dotted line in Figure 11.

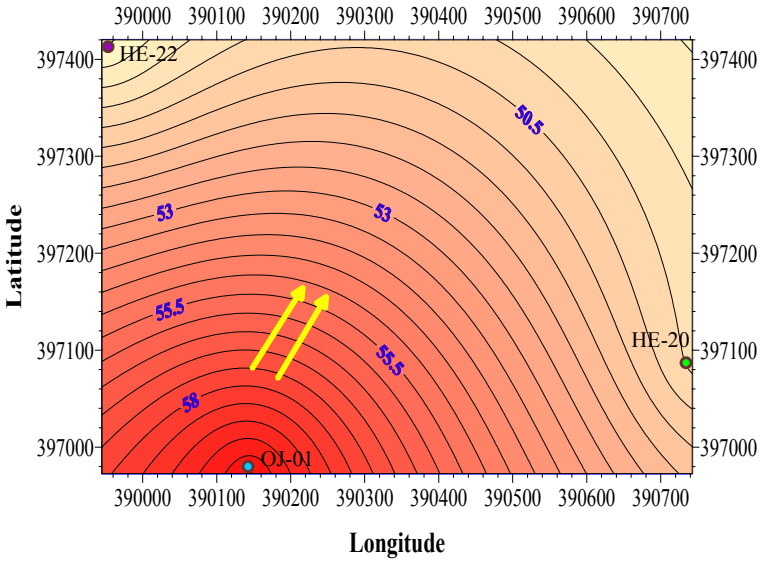

FIGURE 10: Pressure distribution (bars) at 600 m b.s.l.; the yellow arrows show the presumed direction of the pressure transient indicating the most likely direction of fluid flow

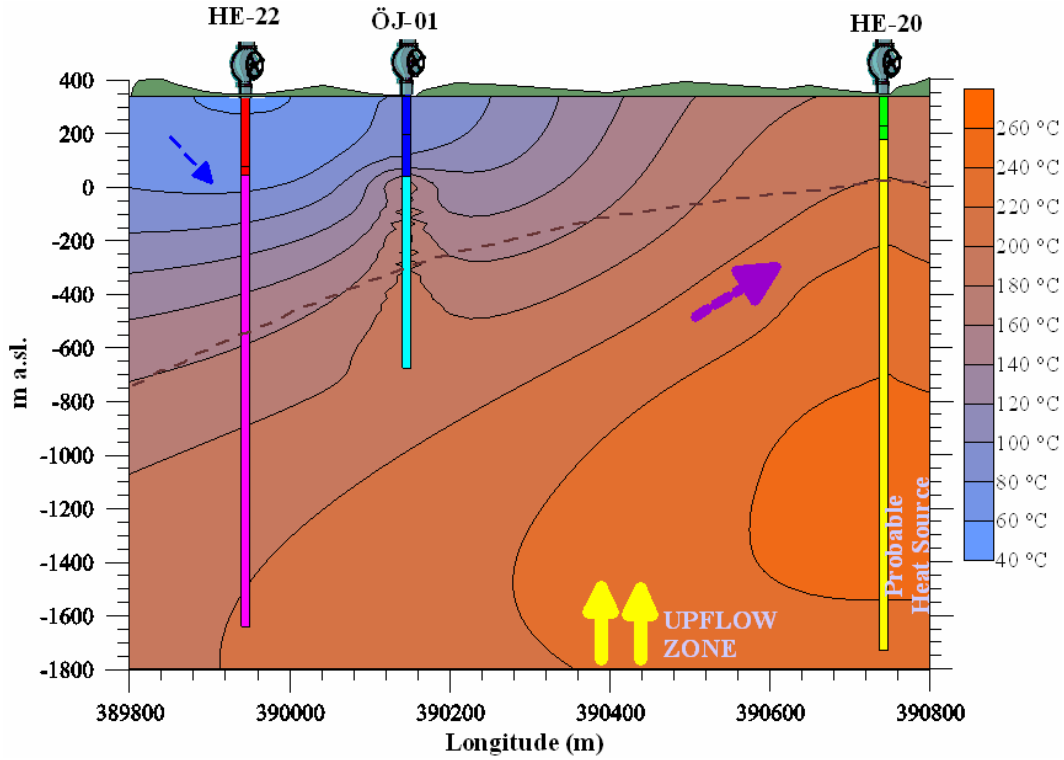

FIGURE 11: Temperature cross-section trending W-E through the Ölkelduháls field and wells HE-20, HE-22 and ÖJ-1; estimate of the cap rock to the dotted line is based on TEM soundings

4. WELL TEST THEORY

4.1 Pressure diffusion equation

The three governing laws that are used in deriving the pressure diffusion equation are as follows:

a) **Law of conservation of mass:**

mass flow in – mass flow out = rate of change of mass accumulation

b) **Darcy's law for radial fluid flow through a porous medium:**

$$q = -2\pi rh\frac{k}{\mu}\frac{\partial P}{\partial r} \tag{1}$$

where q = Volumetric flowrate (m^3/s);
h = Reservoir thickness (m);
k = Formation permeability (m^2);
P = Reservoir pressure (Pa);
r = Radial distance (m);
μ = Dynamic viscosity of the fluid (kg/ms);

c) **The definition of compressibility:**

$$c = \frac{1}{\rho}\left(\frac{\partial \rho}{\partial P}\right)_T \tag{2}$$

where c = Compressibility of the fluid (Pa^{-1});
ρ = Density of the fluid (kg/m^3);
T = Temperature (°C).

Assuming a slightly compressible fluid (i.e. c is constant), laws a-c, gives the following radial pressure diffusion equation:

$$\frac{\partial}{\partial r}\left(\frac{r\partial P(r,t)}{\partial r}\right) = \frac{\mu c_t}{k}\left(\frac{\partial P(r,t)}{\partial t}\right) \tag{3}$$

where $P(r, t)$ = Reservoir pressure at distance r and time t (Pa);
c_t = Compressibility of wet reservoir formation (Pa^{-1}) ;
t = Time (s).

The radial pressure diffusion equation is a partial differential equation that describes isothermal flow of fluid through a porous media and how the pressure $P(r, t)$, diffuses through the reservoir. Initial and boundary conditions are required to solve for $P(r, t)$. For an infinite acting reservoir, the boundary conditions are:

a) Initial conditions:

$$P(r, t) = P_i \qquad \text{for } t = 0,\ r > 0 \tag{4}$$

where P_i = Initial reservoir pressure (Pa).

b) Inner and outer boundary conditions:

$$P(r, t) = P_i \qquad r \to \infty \text{ and } t > 0 \tag{5}$$

$$q = -2\pi rh\frac{k}{\mu}\frac{\partial P}{\partial r} \qquad r \to 0 \text{ and } t > 0 \tag{6}$$

Initially, the reservoir is assumed at rest, P_i. At time zero ($t = 0$) the production well begins discharge at a constant rate q (m^3/s). The pressure in the reservoir, as a function of time, t, and radial distance, r, from the production well is given by assuming an infinitely small well radius and that Darcy's law is valid:

$$P(r,t) = P_i + \frac{q\mu}{4\pi kh} Ei\left(-\frac{\mu c_t r^2}{4kt}\right) \tag{7}$$

Ei is the exponential integral function defined as:

$$Ei(-x) = -\int_x^{\infty} \frac{e^{-u}}{u} du \qquad where \quad x = \frac{\mu c_t r^2}{4kt}$$

For $x < 0.01$: $Ei(-x) \cong \gamma + \ln x$, where $\gamma = 0.5772$ is the Euler's constant.

Therefore, if $t > 100\ \mu c_t r^2/4k$ and $\ln x = 2.303 \log x$, then the solution for the radial pressure diffusion equation can be simplified to:

$$P(r,t) = P_i + \frac{2.303\bar{q}\mu}{4\pi kh}\left[\log\left(\frac{\mu c_t r^2}{4kt}\right) + \frac{\gamma}{2.303}\right] \tag{8}$$

4.2 Semilog analysis

The Theis solution to Equation 3 can be written as:

$$P_i - P(r,t) = \frac{2.303\bar{q}\mu}{4\pi kh}\left[\log\left(\frac{4k}{\mu c_t r^2}\right) - \frac{\gamma}{2.303}\right] + \frac{2.303\bar{q}\mu}{4\pi kh}\log(t) \tag{9}$$

The above equation is in the form $\Delta P = A + m \log(t)$, which is a straight line with slope m on a semilog graph where:

$$\Delta P = P_i - P(r,t);\ A = \frac{2.303\bar{q}\mu}{4\pi kh}\left[\log\left(\frac{4k}{\mu c_t r^2}\right) - \frac{\gamma}{2.303}\right]; \quad and \quad m = \frac{2.303\bar{q}\mu}{4\pi kh} \text{ Pa/log cycle}$$

Thus, when pressure change, ΔP, is plotted against time, t, on a semi-logarithmic scale, (ΔP vs. log t) an asymptotic straight line response for the infinite acting radial flow period of a well should be obtained. This analysis is based on the location and interpretation of the semi-log straight line response that represents the infinite acting radial flow behaviour of the well. When slope, m, is identified, the transmissivity T can be found.

$$T = \frac{kh}{\mu} = \frac{2.303\bar{q}}{4\pi m} \tag{10}$$

If the temperature is known, then the dynamic viscosity, μ, can be obtained from steam tables and, subsequently, the permeability thickness, kh, may then be calculated as follows:

$$kh = \frac{2.303\mu\bar{q}}{4\pi m} \tag{11}$$

The formation storativity or storage coefficient, $S = c_t\, h$, is then obtained from the intercept with the ΔP-axis when the permeability thickness is known. Using the value of the drawdown ΔP at some time t, gives:

$$\frac{\Delta P}{m} = \left\{\left[\log\left(\frac{4kh}{\mu}\right)\left(\frac{1}{S}\right)\left(\frac{t}{r^2}\right)\right] - \frac{\gamma}{2.303}\right\} \tag{12}$$

or

$$10^{\frac{\Delta P}{m}} = \left(\frac{kh}{\mu}\right)\left(\frac{1}{S}\right)\left(\frac{t}{r^2}\right)\left(4x10^{-\frac{\gamma}{2.303}}\right) \tag{13}$$

i.e.

$$S = 2.246T\left(\frac{t}{r^2}\right)x10^{\frac{-\Delta P}{m}} \quad where \quad T = \frac{kh}{\mu} \tag{14}$$

However, as the wellbore has finite volume, it becomes necessary to determine the duration of the wellbore storage effect or the time at which the semi-log straight line begins. The Theis solution for the constant rate drawdown test is based on the assumption that the down-hole production rate or injection rate changes instantaneously from zero to its constant value. However, due to the wellbore storage effect, the fluid flow out of the wellhead is not always the same as the flow from the reservoir into the well. For example, if a pressurized well is suddenly opened, the fluid within the wellbore will expand thereby (temporarily) adding to the flow from the reservoir. Another type of wellbore storage is seen with the injection into a well through a tubing string. As the fluid flows into the well the water level in the annulus (between the well and the tubing string) will rise at the same time as fluid is flowing into the reservoir, thereby causing a temporary addition to the pressure transient. Several other factors can contribute to the wellbore storage effect but the above are the main factors. Therefore, it is important to find the actual beginning to the semi-log straight line. The wellbore storage shows up as a unit slope straight line on a log-log plot of ΔP vs. t. As a rule of thumb, there are about 1½ log cycles between the end of the unit slope straight line representing wellbore storage and the start of the purely infinite acting reservoir response. This 1½ log cycle rule provides a useful method for identifying the start of the semi-log straight line. The wellbore storage coefficient, C (m^3/Pa), is defined as the volume, ΔV, of the fluid that the wellbore itself will produce due to a given pressure drop, ΔP, and is denoted as:

$$C = \frac{\Delta V}{\Delta P} \tag{15}$$

And if a well has fluid with a free surface, the wellbore storage coefficient is estimated by:

$$C = \frac{V_u}{\rho\, g} \qquad \text{or} \qquad C = \frac{\pi r_w^2 h / h}{\rho\, g} = \frac{\pi r_w^2}{\rho g} \tag{16}$$

where V_u = Wellbore volume per unit length (m^3/m);
ρ = Density (kg/m^3);
g = Gravitational acceleration (m/s^2).

But for a completely filled well, the fluid compression storage coefficient, C, is given by:

$$C = c_f V_w \tag{17}$$

where c_f = Fluid compressibility (Pa^{-1});
V_w = Volume of wellbore (m^3).

Typical values of compressibility used are as follows:

Water compressibility at 250°C, $c_w = 10 \times 10^{-10}\ Pa^{-1}$
Basaltic rock compressibility, $c_r = 0.20 \times 10^{-10}\ Pa^{-1}$

Therefore we get:

$$\begin{aligned} c_t &= \left[\phi c_w + (1-\phi)c_r\right] \\ &= \left[\left(0.14 \times 10.0 \times 10^{-10}\right) + \left((1-0.14)(0.20 \times 10^{-10})\right)\right] \\ &= 1.572 \times 10^{-10}\ /\ Pa \end{aligned} \tag{17a}$$

Skin is defined as an additional pressure drop ΔP_{Skin} at the well face. Sometimes, there is a zone surrounding the well that has been invaded by mud filtrate, cement, or cuttings during drilling and completion of the well. In this area, referred to as the skin zone, the permeability is not the same as in the reservoir:

$$\Delta P_{skm} = \frac{\bar{q}\mu}{2\pi kh} s \tag{18}$$

where s = Skin factor (dimensionless)

If the skin factor is negative, the permeability of the skin zone is greater than the reservoir permeability, indicating that the well may have been stimulated. On the other hand, if the permeability in the skin zone is less than reservoir permeability, the skin factor will be positive and the well is damaged. Skin factor can be used to calculate the radius of the skin zone if the permeability of the skin zone, k_s, and the permeability of the reservoir, k, are known:

$$s = \left(\frac{k}{k_s} - 1\right) \ln \frac{r_s}{r_w} \tag{19}$$

Skin has a similar effect as changing the effective radius, r_{wa}, of the wellbore.

$$r_{wa} = r_w e^{-2s} \tag{20}$$

In pumping a well with skin, the total pressure change is given by:

$$\Delta Pt = \Delta P + \Delta Ps = Pi - P(r, t) + \Delta Ps \tag{21}$$

or

$$\Delta P_t = -\frac{2.303\bar{q}\mu}{4\pi kh}\left[\log\left(\frac{\mu c_t r_w^2}{4kt}\right) + \frac{\gamma}{2.303}\right] + \frac{2s\,\bar{q}\mu}{4\pi kh} \tag{22}$$

The presence of skin does not alter the evaluation of transmissivity in semilog analysis. It does affect storativity. Equation 22 must now be written as:

$$c_t H\, e^{-2s} = 2.246T\left(\frac{t}{r_w^2}\right)x10^{\frac{-\Delta P}{m}} \quad where \quad T = \frac{kh}{\mu} \tag{23}$$

In general, the steps involved in a semi-log analysis include the following:

1) Draw a log-log plot of ΔP versus *t;*
2) Determine the time at which the unit slope line representing the wellbore storage ends;
3) The semi-log straight line is expected to start at 1½ log cycles after the unit slope line;
4) Draw a semi-log plot of ΔP versus log *t;*
5) Look for the straight line, starting at the suggested time point;
6) Estimate the transmissivity and storativity depending on the skin effect;
7) Estimate the skin factor s from the intercept of the line using the pressure point at unit time on the straight line (not on the data).

Appendix II demonstrates the use of semilog analysis.

4.3 Dimensionless variables and type curve analysis

Well test analysis often makes use of dimensionless variables in order to simplify the reservoir models by embodying the reservoir parameters such as flowrate, *q,* and permeability, *k*, thereby reducing the total number of unknowns. They have the additional advantage of providing a model solution that is independent of any particular system. The pressure change in a test depends on particular flowrates, permeability, and other parameters. These parameters can be absorbed into the definition of pressure and time to define dimensionless variables:

$$P_D = \frac{2\pi kh}{q\mu}\left(P_i - P(r,t)\right); \qquad t_D = \frac{kt}{c_t \mu r_w^2}; \qquad r_D = \frac{r}{r_w}; \qquad C_D = \frac{5.615C}{2\pi\phi\, c_t h\, r_w^2} \tag{24}$$

Each appropriate reservoir model for a well test is found by plotting pressure transient data from a well test on a log-log graph and comparing it with various type curves. Type curves are dimensionless solutions associated with a specific reservoir model. Generally, the procedure for a type curve analysis can be outlined as follows:

1) The data is plotted as log ΔP vs. log Δt on the same scale as that of the type curve;
2) The curves are then slid, one over the other, while keeping the vertical and horizontal grid lines parallel until the best match is found. Any convenient match can be chosen;
3) The pressure and time values are read from fixed points on both graphs, ΔP_M, P_{DM}, Δt_M, and t_{DM};
4) For an infinite acting system, the transmissivity, *T*, is evaluated as:

$$T = \frac{kh}{\mu} = \frac{\bar{q}}{2\pi}\left(\frac{P_D}{\Delta P}\right)_M \tag{25}$$

5) And the storativity can be estimated by:

$$S = c_t H = \frac{kh}{\mu r_w^2}\left(\frac{\Delta t}{t_D}\right)_M = \frac{T}{r_w^2}\left(\frac{\Delta t}{t_D}\right)_M \tag{26}$$

Type curve matching generally gives approximate results and should not be used for test analysis if semilog analysis techniques can be applied. Appendix II demonstrates the use of type curves analysis.

4.4 Multiple rate testing

Accurate flowrate and pressure measurements are essential for the successful analysis of any transient well test. Rate measurements are much more critical in multiple-rate testing, however, than in conventional, constant-rate well tests. Without good flowrate data, good analysis of multiple-rate tests is impossible. Multiple-rate testing has the advantage of providing transient test data while production/injection continues. It tends to minimize changes in the wellbore storage coefficient and phase segregation (humping) effects and, thus, may provide good results when drawdown or build-up testing would not. Although flowrate may change continuously, it is treated as a series of discrete constant rates for analysis purposes (Earlougher, 1977). The step-wise approximation improves as the time intervals become smaller. Using the log approximation to the line source then:

$$\frac{P_i - P_{wf}}{q_N} = m' \sum_{j=1}^{N} \left[\frac{(q_j - q_{j-1})}{q_N} \log(t - t_{j-1}) \right] + b' \tag{27}$$

is the equation of a straight-line with slope, $m' = \dfrac{2.303\mu}{4\pi kh}$ (Pa/(m^3/s)) and intercept:

$$b' = m' \left[\log\left(\frac{k}{\phi \mu c_t r_w^2} \right) + 0.351378 + 0.86859 s \right] \tag{27a}$$

Once the data plot is made, the straight-line slope and intercept are measured. Permeability and skin factor are estimated from the slope and intercept of the data plot where:

$$s = 1.1513 \left[\frac{b'}{m'} - \log\left(\frac{k}{\phi \mu c_t r_w^2} \right) - 0.351378 \right] \tag{27b}$$

5. ANALYSIS OF WELL TEST DATA

In most cases of well testing, the reservoir response that is measured is the pressure response. Hence, in many cases well test analysis is synonymous with pressure transient analysis. The pressure transient is due to changes in production or injection of fluids, hence we treat the flowrate transient as input and the pressure transient as output.

In well test interpretation, we use a mathematical model to relate pressure response (output) to flow rate history (input). By specifying that the flowrate history input in the model be the same as that in the field, we can infer that the model parameters and the reservoir parameters are the same if the model pressure output is the same as the measured reservoir pressure output. Clearly, there can be major difficulties involved in this process, since the model may act like the actual reservoir even though the physical assumptions are entirely invalid. This ambiguity is inherent in all inverse problems, including many others used in reservoir engineering (e.g., history matching in simulation, decline curve analysis or material balance). However, the dangers can be minimized by careful specification of the well test in such a way that the response is most characteristic of the reservoir parameters under investigation. Thus, in most cases, the design and the interpretation of a well test are dependent on the objectives.

Analysis of well test data forms part of the modelling of flow and transport characteristics of a reservoir which predict the future behaviour of a subsurface flow system. The reliability of such model predictions, however, must be questioned due to the uncertainties in the conceptual model and the input parameters. In most cases a flaw in the model structure leads to considerable prediction

error, making the choice of the conceptual model the most important step in model development. The second largest source of uncertainty stems from insufficient knowledge about the model parameters and their variability. One way to obtain parameter estimates and their uncertainties is to calibrate the model against observations. Since parameters estimated using inverse modelling can be considered optimal for the given model, an unacceptably large fitting residual may indicate the existence of a model structure error. Unfortunately, a good match to the data does not prove that the conceptual model is correct. It could be that the data are not sensitive with respect to certain aspects of the model. If these aspects become relevant during subsequent model application, the predictions may be erroneous despite successful history matching and small parameter uncertainties. This problem is reflected in the statement that all parameter values estimated by data inversion are strictly model-related. This fact can be an advantage when the key aspects of a model are not changed between history matching and prediction runs (Pruess and Finsterle, 1996).

5.1 Reservoir evaluation

To reach a decision on the best production strategy for a given reservoir (or even whether it is worthwhile to spend the money to produce it at all), we need to know its deliverability, properties, and size. Thus, it will be attempted to determine the reservoir permeability-thickness product (*kh*), initial reservoir pressure, and the reservoir boundaries. Furthermore, the pressure transient will be examined in order to evaluate whether well productivity is governed by near wellbore effects (i.e. skin) or by the reservoir at large.

The permeability-thickness (*kh*) governs the ease by which fluids can flow to the well. Hence, it is a parameter that we need to know in order to design well spacing and number of wells. If permeability-thickness is low, we may need to evaluate the cost-effectiveness of stimulation. Reservoir pressure tells us how much potential energy the reservoir contains (or has left) and enables us to forecast how long reservoir production can be sustained. Pressure in the vicinity of the wellbore is affected by drilling and production processes, and may be quite different from the pressure further out in the reservoir. Well test interpretation allows us to infer distant pressure from the local pressure that can actually be measured.

Analysis of reservoir limits enables us to determine how much reservoir fluid is present (be it oil, gas, water, steam or any other) and to estimate whether the reservoir boundaries are closed or open (with aquifer support, or a free surface). The well test data for HE-20 that were analysed came from two tests:

1. A two-rate step fall-off test called step five (5) carried out on 2005-12-11 for approximately 1.3 hours where the injection rate was changed from 50 to 13 l/s. Downhole pressures at 660 m depth during the injection test are shown in Appendix III (Table 2).
2. A two-rate step injection test called step six (6) carried out from 2005-12-15 to 2005-12-17 for approximately 72 hours where the injection rate was increased from 13 to 43 l/s. Downhole pressures at 1386 m depth during the injection test are shown in Appendix III (Table 3).

The injection test data were analysed by using a semi-log plot (Figure 12), Theis type curve

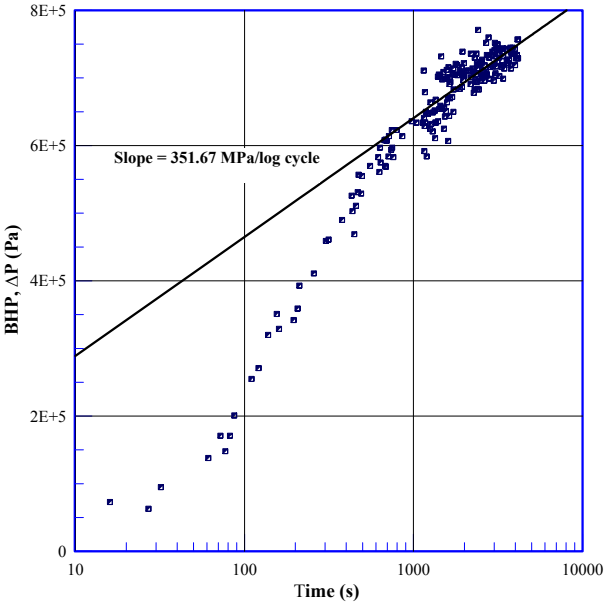

FIGURE 12: Semilog plot for two-rate step injection test (5)

matching methods (Figure 13), multirate techniques (Figures 14 and 15) and the non-linear regression and pressure derivative method (Figure 16) in order to calculate the transmissivity, permeability-thickness, skin and formation storage for the well. A summary of the results is given in Table 2.

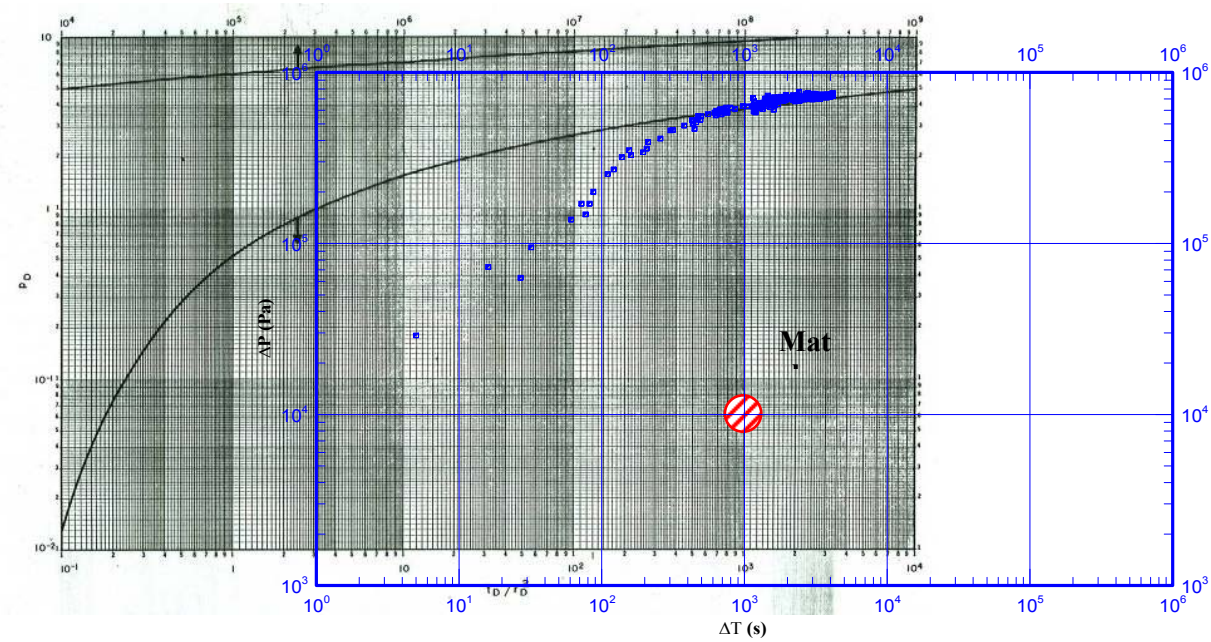

FIGURE 13: Type curve matching, test five; here the actual data was matched to the exponential-integral solution type curve. The type curve does not include wellbore storage and skin, hence, transient pressure from the infinite acting period (of a single well) is matched to the dimensionless pressure of the type curve (Earlougher, 1977)

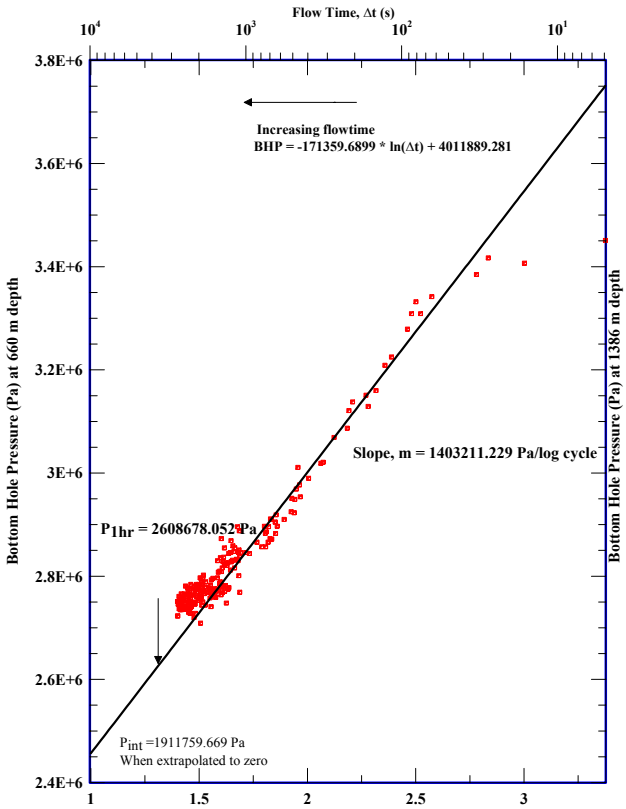

FIGURE 14: Two-rate injection test data plot for rate reduction; step test five (5)

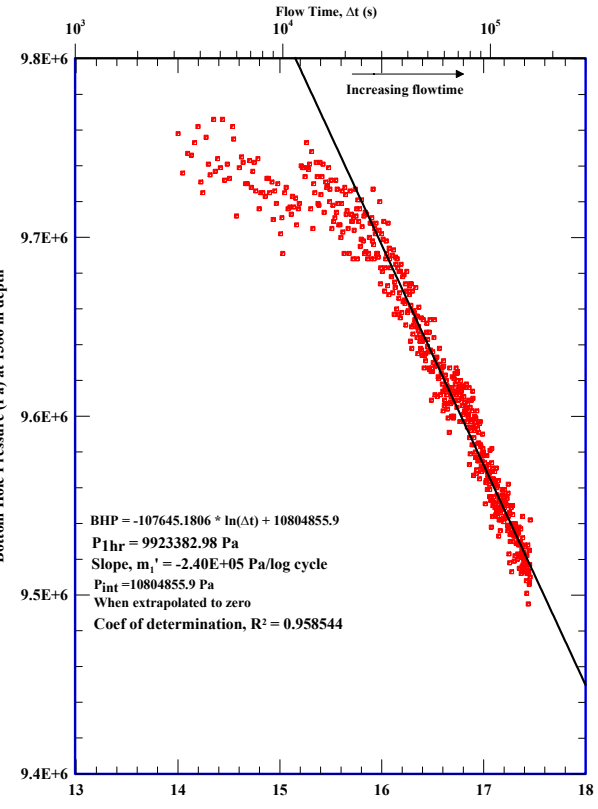

FIGURE 15: Two-rate injection test data plot for rate increase; step test six (6)

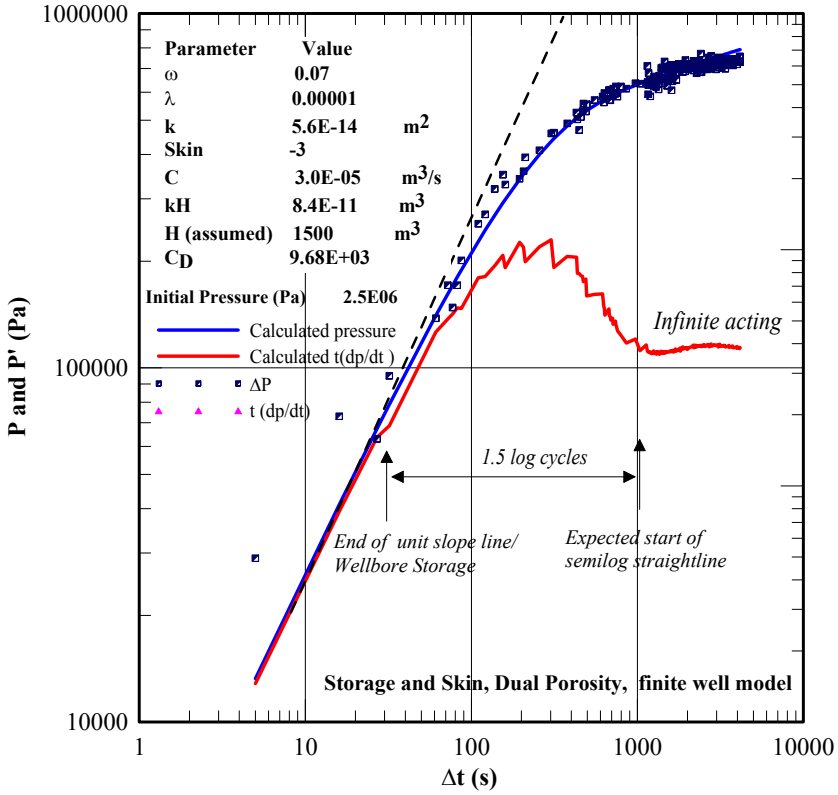

FIGURE 16: The derivative plot for injection

TABLE 2: Summary of well test analysis results for well HE-20 in the Ölkelduháls reservoir

Type of test	Flowrate (l/s)	Method of analysis	Perm. thickn., *kh* (Dm)	Skin	Storativity (m/Pa s)	Storage coefficient (m^3/s)
Two-rate step fall-off test (5)	37 (Δq)	Semilog (Theis solution)	25	-1.8	8.3×10^{-5} affected by skin	4.78165×10^{-6}
	37 (Δq)	Theis type curve	48		2.4×10^{-6}	N/A
	-13 (down from -50)	Multi rate	9	-0.1	-	-
	-13 (down from -50)	Non-linear regre. analysis & press. derivative	84	-3.0	3.3×10^{-8}	3.0×10^{-5}
Two-rate step injection test (6)	-43 (up from -13)	Multi rate	13	-1.4	–	–
Range			**9 to 84**	**-3 to -0.1**	**Variable**	
Comparison with other analyses from the Hellisheidi geothermal area (well HE-4, 12/10/2001)						
			kh/μ			
Injection	20.7	Lokur*	5×10^{-8}	-1.7	1.2×10^{-8}	
Injection	30.6	Lokur*	8×10^{-8}	-1.9	7.5×10^{-8}	

*Lokur is a computer program used to calculate wellbore parameters from well tests; it uses nonlinear regression to fit conceptual models to the raw data by altering parameters such as transmissivity, storativity, wellbore storage and skin;
NB: In two-rate well test analysis, constant flowrate is assumed from time 0 to time t_1, at the start of the test when the transient data is measured (i.e. flowrate q_2, bottom-hole pressure etc).

5.2 Two-rate tests

Injectivity testing - pressure transient testing during injection into a well at constant or variable injection rates - was carried out for well HE-20 at two rates; the pressure data during the second rate q_2 are shown in Figures 14 and 15. When a multiple-rate test consists of only two flowrates, both testing and analysis are simplified (Earlougher, 1977). The two-rate tests provide information about k and s while production continues. Wellbore storage effects are often thought to be minimized or eliminated by two-rate tests. In fact, wellbore storage effects last just about the same amount of time in a two-rate test as in a normal build-up, draw-down/fall-off test. However, a two-rate test often can be used to prevent wellbore storage increase, thus providing an analyzable test when one might not be sufficient. The main advantage of a two-rate test, over say, a build-up test, is that deferred production is minimized. Either a decreasing or increasing rate sequence may be used. Equation 27 may be modified to the form presented by Russell for a two-rate test:

$$P_{wf} = m_1' \left[\log\left(\frac{t_1 + \Delta t}{\Delta t} \right) + \frac{q_2}{q_1} \log \Delta t \right] + P_{\text{int}} \tag{28}$$

A constant flowrate is assumed from time 0 to t_1, at the start of the test and reservoir permeability may be estimated from the slope of the data plot's straight line:

$$m_1' = \frac{2.303 q_1 \mu}{4\pi k h} \tag{28a}$$

However, the skin factor is estimated from:

$$s = 1.1513 \left[\frac{q_1}{q_1 - q_2} \left(\frac{P_{wf}(\Delta t = 0) - P_{1hr}}{m_1'} \right) - \log\left(\frac{k}{\phi \mu c_t r_w^2} \right) - 0.351378 \right] \tag{29}$$

The intercept of the data plot may be used to estimate the false pressure, P^* which is used to estimate average reservoir pressure:

$$P^* = P_{\text{int}} - \left[\frac{q_1}{q_1 - q_2} \left(P_{wf}(\Delta t = 0) - P_{1hr} \right) \right] \tag{29a}$$

Other parameters were assumed or estimated as follows:

T (cold water) injected	10°C
c_t for typical basalt matrix at T reservoir (250°C)	1.57×10^{-10} Pa^{-1}
Average porosity, φ	14%
r_w	1.22×10^{-1} m
Reservoir thickness, H (assumed)	1500 m

	Step test 5	**Step test 6**	
t_1	7800	259,200	s
q_1	-5.00×10^{-2}	-1.30×10^{-2}	m^3/s
q_2	-1.30×10^{-2}	-4.30×10^{-2}	m^3/s
μ	1.30×10^{-2}		Pa s
Slope, m_1'	1.40×10^{6}	2.40×10^{5}	Pa / log cycle
$P_{wf}(\Delta t = 0)$	4.01×10^{6}	9.70×10^{6}	Pa
P_{int}	1.91×10^{6}	1.08×10^{6}	Pa
P_{1hr}	2.61×10^{6}	9.92×10^{6}	Pa
Depth of gauge	660	1600	m

Permeability thickness of 8.49 Dm and skin of -0.14 were estimated using Equations 28a and 29 for step test five where injection was reduced from 50 to 13 l/s.

Similarly when the rate was increased from 13 to 43 l/s in injection test 6, the permeability-thickness was estimated to be about 13 Dm and the skin was found to be -1.44, as summarised in Table 3.

TABLE 3: Results from step tests 5 and 6 on permeability thickness and skin factor

Parameter	**Step test 5**	**Step test 6**
Transmissivity (m^3/Pa s)	6.53×10^{-9}	9.93×10^{-9}
Permeability thickness, *kh* (m^3)	8.49×10^{-12}	1.29×10^{-11}
Skin factor	-0.14	-1.44
False pressure (Pa)	1.55×10^{4}	1.07×10^{7}

5.3 Dual porosity behaviour

Discussion in previous sections has been focused on reservoirs with homogeneous properties. Because of the diffusive nature of pressure transmission many reservoirs do indeed behave as if they were homogeneous, even though it is certain that the reservoir properties must be non-uniform to some extent. However, there is a type of reservoir heterogeneity that is noticeable in pressure transients in reservoirs that have distinct primary and secondary porosities. These pressure effects are known as dual porosity or double porosity behaviour and are quite commonly seen, particularly in naturally fractured reservoirs such as Ölkelduháls.

In a dual porosity reservoir, a porous "matrix" of lower transmissivity (primary porosity) is adjacent to higher transmissivity medium (secondary porosity). Thin stratigraphic sequences of differing permeability can also give rise to dual porosity effects. Although there are variations, a common model is to associate fluid storativity with both the fractures (secondary porosity) and the matrix (primary porosity), but to assume transmissivity mainly in the fractures. In such a dual porosity model, fluid flows to the wellbore through the fractures alone, although it may feed from the matrix blocks into the fractures.

The dual porosity effects are described in terms of two parameters that relate primary and secondary properties. The first of the two parameters is the storativity ratio, ω, that relates the secondary (or fracture) storativity to that of the entire system:

$$\omega = \frac{\left(\phi_f \; c_{tf}\right)}{\left(\phi_f \; c_{tf} + \phi_m \; c_{tm}\right)}$$

Whereas the second parameter depends on the transmissivity ratio, and is designated as:

$$\lambda = \alpha \frac{k_m}{k_f} r_w^2$$

where α = A/xV is factor that depends on the geometry of the inter-porosity flow between the matrix and fractures;
A = The surface area of the matrix block (m^2);
V = The matrix volume (m^3); and
x = A characteristic length related to size and shape of conceptual matrix blocks (m).

Values of ω can be less than or equal to one. It is normal practice to assume ω equal to one - a classic case of reservoir homogeneity. In naturally fractured reservoirs, ϕ_f is usually very small, however, the large fracture compressibility c_{tf} means that ω is commonly less than 0.1, but not necessarily many

orders of magnitude less. Values of λ are usually very small, on the order of 10^{-3}-10^{-10}. If the value of λ is larger than 10^{-3}, the level of heterogeneity is insufficient for dual porosity effects to be of importance, and again the reservoir acts as a single porosity.

5.4 Non-linear regression and the derivative plot

Also known as automated type curve matching, non-linear regression is entirely different from graphical techniques in that it uses a mathematical algorithm to match the observed data to a chosen reservoir model. The matching is achieved by changing the values of the unknown reservoir parameters (such as permeability, skin, ω, λ, distance to boundary, etc.) until the model and the data fit as closely as possible (in a least-squares sense) by minimizing the sum of squares of the differences between measured pressure and model pressure. Data from HE-20 was fitted to a finite well, dual porosity model with storage and skin. The mathematical fitting process allowed for the statistical determination of goodness of fit, thus providing not only a numerical answer but also a quantitative evaluation of how good the answer is. This method of analysis is capable of estimating reservoir parameters from pressure responses that are in the transition regions which cannot be interpreted directly by graphical methods.

The derivative plot provides a simultaneous presentation of "log ΔP vs. log Δt" and "log ($t\,\partial P/\partial t$) vs. log t" (Horne, 1995). The advantage of the derivative plot is that it is able to display in a single graph many separate characteristics that would otherwise require different plots.

5.5 Estimating dual porosity parameters on derivative plots

The derivative plot provides a much more practical method for estimating ω and λ. The position of the minimum in the derivative (the "dip" that characterizes dual porosity behaviour) completely defines the values of both ω and λ (as described by Horne, 1995). The minimum in the derivative can be shown to lie at a dimensionless pressure derivative value of:

$$\left(t_D \frac{\partial P_D}{\partial t_D} \right)_{min} = \frac{1}{2}\left(1 + \omega^{\frac{1}{1-\omega}} - \omega^{\frac{\omega}{1-\omega}} \right) \tag{30}$$

and with a dimensionless time value of:

$$\left(t_D\right)_{min} = \frac{\omega}{\lambda}\ln\frac{1}{\omega} \tag{30a}$$

The value of ω is then evaluated by solving Equation 30 iteratively using the Newton-Raphson method, after which λ can be found directly from Equation 30a. Figure 16 shows the derivative plot from a well test in a fracture-dominated reservoir which is assumed to exhibit dual porosity characteristics. The location of the minimum is at a pressure value of 2799 Pa and a time value of 3988.9 seconds. Using known values of q, B=1 (for water), m and H, together with a previously estimated value of k, the dimensionless pressure derivative at the minimum can be calculated, after which the first estimate of ω is found from:

$$\log\omega \approx \left[0.01765 + \log\left(t_D \frac{\partial P_D}{\partial t_D} \right)_{min} \right] \Big/ 0.94903$$

A final estimate of ω is found by Newton-Raphson as described earlier. After estimating ω, the dimensionless time value at the minimum can be calculated using known values of ϕ, μ, c_t and r_w together with the estimated value of k, after which λ can be estimated using Equation 30a. This also

requires the inclusion of the recent estimate of ω. Some of the analytical equations involved in estimating permeability-thickness, transmissivity, skin and storage in the model used above are presented in Appendix II.

5.6 Reservoir boundary response

When a well is being tested the radial flow period does not last indefinitely, instead the effects of the reservoir boundaries are felt eventually. The time at which the boundary effect is noticed is dependent on several factors, including the distance to the boundary, the properties of the permeable formation and the fluid that fills it. The two types of reservoir boundaries that are most commonly considered are (a) impermeable and (b) constant pressure. An impermeable boundary (also known as a closed boundary, see Figure 17) occurs where the reservoir is sealed and no inflow occurs. No flow boundaries can also arise due to the interference between wells. A constant pressure boundary rarely occurs in practice. However, in many cases aquifer support, a balanced injection pattern or the presence of a large gas cap can cause an effect that closely approximates a constant pressure boundary. Figure 17 shows typical pressure responses for different models.

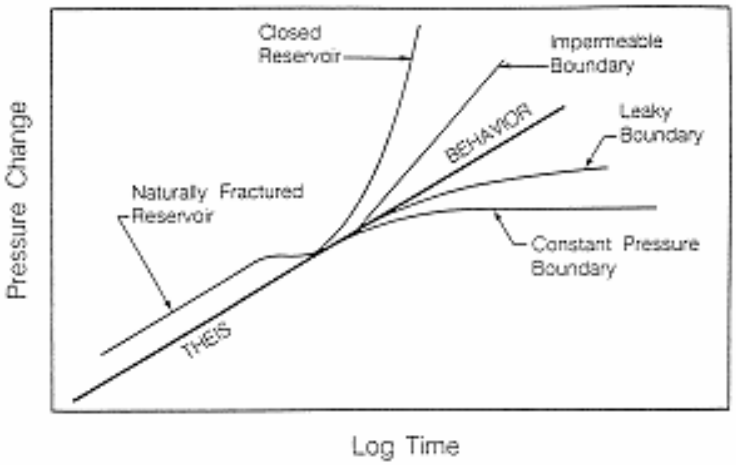

FIGURE 17: Typical pressure responses for different reservoir models

Thermal effects in the fluid and the surroundings of the wellbore can often cause difficulties in interpreting boundary effects. For example, the aperture of a fracture intersecting the well can increase during injection because of thermal contraction of the rock as the wellbore cools down (Egill Júlíusson, 2006, pers. comm.).

5.6.1 Radius of investigation

Pressure response follows a diffusion type of response which implies that a pressure change at the well is felt at least infinitesimally everywhere in the reservoir. However, from a practical standpoint, there will be points at some distance from the well at which the pressure response will be so small as to be undetectable. The closest such point defines the region of the reservoir that has been "tested" during a well test, and we may refer to the distance to this point as the radius of investigation. However, it is better to acknowledge that the radius of investigation is at best a vague concept that should only be used in a qualitative manner (Horne, 1995).

One way to think about the radius of investigation is in terms of the time to a pseudo-steady state. A reservoir with closed boundaries could be assumed to be circular and the boundary effect (pseudo-steady state) will be reached in a dimensionless time t_{DA} of 0.1. If no boundary effect has been seen at a particular time during a test, then the dimensionless time t_{DA} for the radius of investigation at that moment must be less than 0.1. This is the basis of the definition described by Van Poollen (Horne, 1995).

In the fall-off test data set used for analysis, there was no evidence of any pressure transient caused by boundary effect. If the test had been conducted for a longer time the pressure transient response at the well would reflect reservoir conditions at greater radius. For a closed circular reservoir, the boundary

response begins at a dimensionless time t_{DA} of 0.1. Given that no such response was observable in the data, we can ascertain that t_{DA} at time t = 1.27 hours (the last data point measured) must be smaller than 0.1. From this we can determine that the radius of investigation was less than the actual radius of the reservoir. Putting this into numbers using data of the step rate fall-off test and the values obtained from Equation 17b and semilog analysis, for a testing duration of 1.27 hours, the area and radius of investigation can be determined from:

$$t_{DA} = \frac{kt}{\phi \mu c_t A} < 0.1$$

$$\frac{\left(25 \times 10^{-12}\right)\left(1.267 \times 3600\right)}{\left(0.14\right)\left(1.3 \times 10^{-3}\right)\left(1.572 \times 10^{-10}\right)A} < 0.1 \qquad (30b)$$

$$Area,\ A > 39.8\ km^2\ and\ r_e > 3.56\ km$$

From this estimate of the radius of investigation, we do not know where the actual reservoir boundaries are in the approximately 20 km^2 area estimated by TEM, but we have determined that they are at least 3.6 km away. We have therefore been able to place an approximate lower bound on the reservoir size. However, it should be emphasized that this radius of investigation is a rather broad estimate of how far the test "sees" into the reservoir - the time at which the well pressure begins to be affected by the boundary may not be within the time limit available to the interpreter for noticing the effect. It is possible that the reservoir could have a boundary closer than 3.6 km, but that its influence is not strong enough to be noticeable. In practice, it is expedient to assume that the lower boundary of reservoir size is rather smaller than the radius of investigation.

6. DELIVERABILITY

The production of steam and water from a geothermal reservoir depends on the reservoir pressure, the flow of fluid through the feedzone into the well, and then up the wellbore to the surface. These three elements of deliverability are called reservoir performance, inflow performance, and wellbore performance, respectively. An output test of a geothermal well gives the deliverability at the time of testing. After a few years of production the deliverability is likely to change because of drawdown in reservoir pressure. The prediction of reservoir pressure with time is one of the subjects of reservoir modelling.

To describe a well's deliverability and have the quantitative data suitable for both reservoir analysis and surface plant design purposes, the following basic information is needed: (a) the total mass flow, (b) the discharge enthalpy, (c) the non-condensable gas content, and (d) the amount of dissolved solids. From (a) and (b) we can calculate (e) the total heat flow, (f) the separated water flow and (g) the separated steam flow. The flow is required as a function of wellhead pressure, P_0 and time. The two parameters chosen depend on the measurement system being used.

Two basic types of flow tests may be done. One is called a discharge test in which flow characteristics are measured at varying pressure over a short period (hours - days). Alternatively, a "rundown", transient or production test may be performed. This involves holding pressure or flow constant and monitoring the changes in pressure or flow over time for months or years. This is the case with a well such as HE-20 which has only recently been discharged and has not yet stabilised. The online data obtained from such a well constitute an output test.

The discharge measurement technique employed at well HE-20 in the Ölkelduháls field involves separation of the steam-water mixture into a flow of water and a flow of steam from a separator (silencer) at atmospheric pressure. The separated water then flows into a V-shaped weir box where its

height is measured. The steam-water flow is determined using the critical lip pressure method with two-phase flow entering the silencer. This technique is referred to as the Russell-James critical lip pressure method. It is based on an empirical formula developed by James (Grant et al., 1982). Although not quite as accurate as the tracer test method, it maintains the use of a minimum of hardware and instrumentation to obtain good results. Analysed data were obtained from Reykjavik Energy - the company that owns the field. Figures 18 and 19 show measured parameters and output characteristics for HE-20, with the grey rows representing data from tracer tests.

Measured values

Date	Time	WHP Po [barg]	Orifice d [mm]	Lip pipe diameter [mm]	Critical lip pressure Pc [barg]	Weir box Water height [mm]	Separation press. [barg]
04/05/2006	13:00	10.50	100	161	0.50	195	0.00
18/05/2006	10:20	11.00	100	161	2.50	190	0.00
30/05/2006	00:00	11.20	100	161	1.26	210	0.00
01/06/2006	13:50	12.00	100	161	1.60	195	0.00
09/06/2006	11:20	12.00	100	161	1.70	195	0.00
19/06/2006	15:35	12.00	100	161	1.40	195	0.00
23/06/2006	15:32	12.00	100	161	1.50	195	0.00
29/06/2006	12:25	11.00	100	161	1.50	180	0.00
07/07/2006	11:24	11.50	100	161	1.50	200	0.00
17/07/2006	10:50	12.20	100	161	1.50	200	0.00
25/07/2006	15:22	11.00	100	161	1.60	195	0.00
28/07/2006	15:05	11.00	100	161	1.20	195	0.00
09/08/2006	14:05	10.50	100	161	1.60	195	0.00
10/08/2006	16:30	10.20	100	161	1.40	200	0.00
23/08/2006	09:38	10.00	100	161	2.00	195	0.00
24/08/2006	17:39	12.00	100	161	1.10	195	0.00
29/08/2006	00:00	11.50	100	161	1.27	211	0.00
31/08/2006	17:39	13.00	100	161	1.30	197	0.00
08/09/2006	14:14	13.00	100	161	1.40	195	5.50
14/09/2006	13:40	15.00	75	100	2.40	175	8.40
29/09/2006	14:49	14.00	75	100	2.40	180	8.00

FIGURE 18: Measured parameters from HE-20 used in the critical lip pressure method of discharge analysis

Calculated values

Water flowrate [l/s]	Enthalpy [kJ/kg]	Total flow [kg/s]	Steam flow [kg/s] [@1bar-a]	Steam flow ap sep. Press [kg/s]	Steam fraction at sep. Pressur [%]
22.88	936.63	29.65	6.80	6.75	22.77
21.46	1476.41	40.31	18.89	18.83	46.71
27.48	1059.00	38.30	10.86	10.80	28.20
22.88	1254.96	36.29	13.44	13.39	36.89
22.88	1277.78	36.88	14.03	13.98	37.90
22.88	1206.80	35.10	12.25	12.20	34.76
22.88	1231.31	35.70	12.85	12.80	35.84
18.77	1357.11	32.07	13.33	13.28	41.42
24.36	1191.91	37.00	12.67	12.62	34.09
24.36	1191.91	37.00	12.67	12.62	34.09
22.88	1254.96	36.29	13.44	13.39	36.89
22.88	1154.96	33.91	11.06	11.00	32.46
22.88	1254.96	36.29	13.44	13.39	36.89
24.36	1167.58	36.40	12.07	12.02	33.02
22.88	1341.76	38.65	15.80	15.75	40.74
22.88	1127.51	33.31	10.46	10.40	31.24
27.79	1053.04	38.60	10.84	10.78	27.94
23.47	1165.61	35.02	11.58	11.53	32.93
22.88	1206.80	35.10	12.25	8.80	25.06
17.50	992.53	23.43	5.95	2.81	11.97
18.77	951.99	24.53	5.79	2.53	10.31

FIGURE 19: Output characteristics for HE-20 estimated by the Russell-James method

Assuming that we have a fairly large amount of steam/water mixture flowing at sonic velocity through an open-ended pipe to the atmosphere, the absolute pressure at the extreme end of the pipe is then proportional to the mass flow rate and enthalpy. Russell-James deduced that:

$$\frac{W_t H_t^{1.102}}{A P_{lip}^{0.96}} = 1680 \quad (31)$$

where P_{lip} = Lip pressure at the end of the pipe (MPa);
W_t = Total mass flowrate (kg/s);
A = Discharge/lip pipe area (cm^2);
H_t = Total fluid enthalpy (kJ/kg).

The water flow W_w (kg/s) from the silencer is related to the total mass flow by the flash correction factor, thus:

$$\frac{W_w}{A\,P_{lip}^{0.96}} = \frac{1680}{H_t^{1.102}} \frac{(H'_s - H_t)}{H_{sw}} \tag{32}$$

where H'_s and H'_{sw} are evaluated at separation - atmospheric pressure. At 100 kPa (near sea level):

$$\frac{W_w}{A\,P_{lip}^{0.96}} = Y = \frac{0.74\,(2675 - H_t)}{H_t^{1.102}} \tag{32a}$$

H_t is then determined by iteration from the above equation. Values range between 400 and 2800 kJ/kg as a function of Y with an accuracy of 1.5% (Grant et al., 1982):

$$H_t = \frac{2675 + 365\,Y}{1 + 3.1\,Y} \tag{33}$$

Thus the James's method consists of measuring the lip pressure, *Pc*, water flow from the silencer, finding the enthalpy of the flow from Equation 32a and calculating the mass flow by correcting for the flash to atmospheric pressure:

$$X = \frac{H_t - H_w}{H_s - H_w} \tag{34}$$

where X = Steam mass fraction as ratio;
H_w = Specific enthalpy of water (kJ/kg);
H_s = Specific enthalpy of steam (kJ/kg).

The deliverability characteristics of well HE-20 are shown in Figures 20 and 21. The maximum total flow at the wellhead used later was estimated using the wellbore simulator discussed in the proceeding sections by assuming atmospheric wellhead pressure.

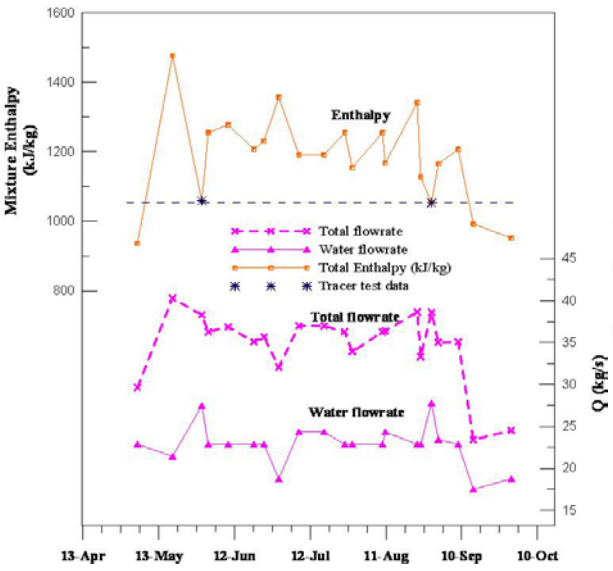

FIGURE 20: First year of flowrate and enthalpy in well HE-20, Ölkelduháls field

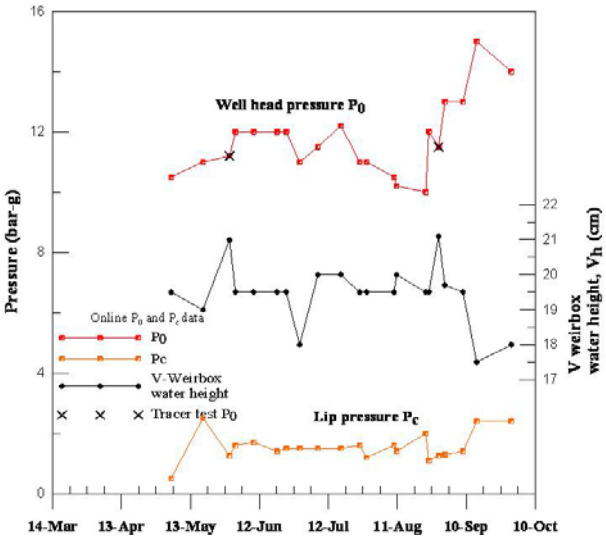

FIGURE 211: Wellhead and lip pressures for well HE-20 over a period of five months

6.1 Discharge analysis and wellbore simulation

Well HE-20 is a two-phase geothermal well with a liquid feed and its deliverability curve can be estimated using the discharge analysis method presented by Gudmundsson (1984). The method is based on using a two-phase flow wellbore simulator such as the computer program HOLA in the ICEBOX software package (Björnsson et al., 1993; Arason et al., 2003), the pressure profile pivot point during initial warm-up, and the concept of productivity index, or some other inflow function.

The discharge analysis method is based on three key elements. The first of these is having a wellbore simulator for two-phase geothermal wells. This makes it possible to calculate down-hole flowing pressures corresponding to measured wellhead conditions. The simulator must have the capability to start the calculations from both the wellhead and wellbottom - only a few simulators have this capability. The second key element is the concept of inflow performance; i.e., the flow of fluid from the reservoir and into the wellbore. If the flow is laminar (Darcy flow), the well known productivity index, *PI,* can be used:

$$PI = (W/(P-P_{wf})$$

where W represents the total wellbore flowrate and P and P_{wf} denote the average reservoir pressure (static feedzone pressure) and wellbottom flowing pressure, respectively. The productivity index is assumed to stay constant not only with flowrate but also with time. However, the average reservoir pressure can change with time. The wells are assumed to have reached steady flowing conditions when measured. Also, the method refers to the well discharge curve at the time of the deliverability measurement used.

The third key element in the discharge analysis method is the pressure at the pivot point depth. The pivot point pressure represents the static reservoir pressure at the well's main feedzone. To obtain the pivot point pressure, at least two pressure surveys must be made in the well during warm-up. The pivot point depth is the only point in the well where the pressure remains constant during warm-up (Grant et al., 1982).

In wells with one major feed zone, the pivot point and the feed zone are at the same depth. In wells with two major feed zones, the pivot point will be located between the feed zones according to the lever rule, and closer to the higher productivity index feed zone.

A summary of the data required for discharge analysis using a wellbore simulator is as follows:

a) One discharge measurement giving total flowrate, wellhead pressure, and total mixture enthalpy. The fluid chemistry should also be included to obtain the liquid density and the amount of non-condensable gases;
b) Two pressure profiles in the static well during warm-up to determine the pivot point that represents the average reservoir pressure at that depth;
c) Well and casing design for depth, diameter, and roughness;

The following calculations are carried out in the discharge analysis method using a wellbore simulator:

a) Starting from the wellhead, calculate the flowing pressure profile down to the pivot point depth. This gives $P_{wf,}$ the flowing wellbore pressure;
b) Calculate the productivity index using the measured flowrate W and the pressure values P and P_{wf} already obtained;
c) Using the productivity index determined, calculate the flowing wellbore pressure for some new flowrate, higher or lower;
d) Starting from the pivot point depth and using the new wellbore flowing pressure, calculate the pressure (and temperature) profile for the wellhead. This gives a new wellhead pressure.

Repeating steps (c) and (d) of the calculations, it becomes possible to determine the wellhead pressure at different flowrates, and to construct an output/deliverability curve.

6.1.1 The HOLA wellbore simulator

The wellbore simulation program HOLA was used for well HE-20 to model the wellbore conditions that influence transport of fluid from the reservoir to the surface. The simulator numerically solves a set of differential equations that describe the steady-state energy, mass and momentum flow in a vertical pipe for single- or two-phase flow. The governing steady-state differential equations for mass, momentum and energy fluxes in a vertical well are according to Björnsson et al. (1993):

$$\begin{aligned} &\frac{dW}{dz} = 0 \\ &\frac{dP}{dz} - \left[\left(\frac{dP}{dz} \right)_{fri} + \left(\frac{dP}{dz} \right)_{acc} + \left(\frac{dP}{dz} \right)_{pot} \right] = 0 \\ &\frac{dE_t}{dz} \pm Q = 0 \end{aligned} \tag{35}$$

where W = Total mass flow (kg/s);
P = Pressure (Pa);
E_t = Total energy flux in the well (J/s);
z = Depth coordinate (m);
Q = Ambient heat loss over unit distance (W/m).

The plus and minus signs indicate downflow and upflow, respectively. The pressure gradient is composed of three terms: wall friction, acceleration of fluid and change in gravitational load over depth interval (*dz*). The governing equation of flow between the well and the reservoir is:

$$W_{feed} = PI \left[\frac{k_{rw}\rho_w}{\mu_w} + \frac{k_{rs}\rho_s}{\mu_s} \right] * \left(P_r - P_{well} \right) \tag{36}$$

where W_{feed} = Feedzone flowrate (kg/s);
PI = Productivity (or injectivity) index of the feedzone (m^3);
k_r = Relative permeability of the phases (subscripts *w* for liquid and *s* for steam);
μ = Dynamic viscosity (Pa.s);
ρ = Density (kg/m^3);
P = Pressure (Pa) subscripts *r* for reservoir.

The dynamic profiles were simulated by varying the number of feed zones, flowrate, and enthalpy contribution of each feed zone and the total enthalpy at wellhead, at a wellhead pressure of 11.2 bar-a, using the wellbore simulator HOLA. The data used was taken from a long-term production test that has been on-going for well HE-20 since March 2006. The well's discharge history for 198 days was analysed. Enthalpy of the well was simulated by HOLA (Figure 22); the enthalpy was also obtained from tracer test data.

6.2 Interpretation of deliverability data

Using online discharge measurements from well HE-20 (a period of 198 days), the temperature and pressure profiles of the March 16, 2006 logs, and data obtained during two tracer tests, deliverability characteristics were deduced with the James critical lip method and wellbore conditions simulated with the Hola program in order to find the heat losses inside the well. The dynamic profiles were simulated by varying the number of feed zones, flowrate, and enthalpy contribution of each feed zone

and the total enthalpy at wellhead of 11.2 bar-a, using the wellbore simulator HOLA. The model results are presented in Appendix III (Table 1).

In a liquid-dominated reservoir of constant temperature and gas content, variations in deliverability are controlled solely by variations in wellhead pressure and the reservoir pressure, otherwise enthalpy and mass flow variations must also be considered.

Feedzone	Depth (m)	Flow (kg/s)	Enthalpy (kJ/kg)	Pressure (bar-a)
Top	0			
1	1400	20	1070	84.8
2	2000	18.3	1129.74	131.6

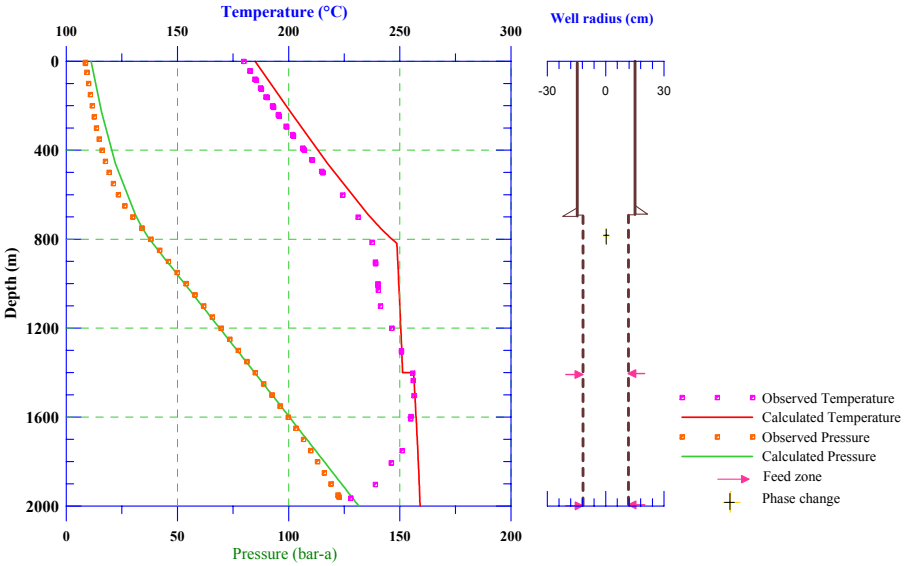

FIGURE 22: Wellbore simulation of pressure transient data and bottomhole temperature in HE20 (logged on March 16, 2006) using the HOLA wellbore simulator and output characteristics from tracer test done in May 2006

6.2.1 Mass flow

From the results of wellbore simulation, the enthalpy (and probably gas content) does not vary greatly. Water enters the well and flashes at about 800 m depth which is some distance up the wellbore.

6.2.2 Maximum discharging pressure

Flow from a well depends on its discharge enthalpy. At low flowrates resistance to flow in either the reservoir or the wellbore becomes unimportant and the flow depends only on the reservoir pressure and discharge enthalpy. By throttling the well the maximum discharging pressure, MDP, that can be attained is determined.

A simple correlation between MDP and discharge enthalpy deduced by Russell-James assumes that the reservoir contains liquid water at boiling point for depth and uses a homogenous flow model where $T = 100P^{0.283}$ (Grant et al., 1982). The MDP for well HE-20 was not measured, but extrapolation of the deliverability curve indicates about 16 bar-a, and using James' equation, implies a feed temperature of 219°C. The corresponding enthalpy of liquid water at this temperature is 939 kJ/kg. The measured discharge enthalpy at a total flow of 38.3 kg/s is 1059 kJ/kg. It increases with increasing flow to about 1400 kJ/kg. The difference 120 kJ/kg is accounted for by the gain in enthalpy after flashing occurs and the fact that the flow model used is homogenous.

Downhole measurements and simulation indicate two feed points, the more dominant one at 1400 m. A maximum temperature of about 256°C is attained at this depth corresponding to an MDP of 27.7 bar-a, and a liquid water enthalpy of 1115.2 kJ/kg. At a reservoir pressure of about 85 bar-a associated with this depth, the enthalpy is 1114.8 kJ/kg.

6.2.3 Enthalpy variations

The discharge enthalpy of a well and any variation with flow (or WHP), define the type of reservoir fluid. The enthalpy curve in Figure 23 corresponds to a reservoir of liquid water, but at some flow rates there is sufficient drawdown for flashing to begin in the formation near the well. A little additional enthalpy is thus gained as was discussed by Menzies et al. (1982).

6.2.4 Cycling and instability

The discharge from well HE-20 is not steady but varies periodically, a characteristic known as cycling, associated with the presence of two significant feeds of different enthalpies to the well.

6.2.5 Productivity index

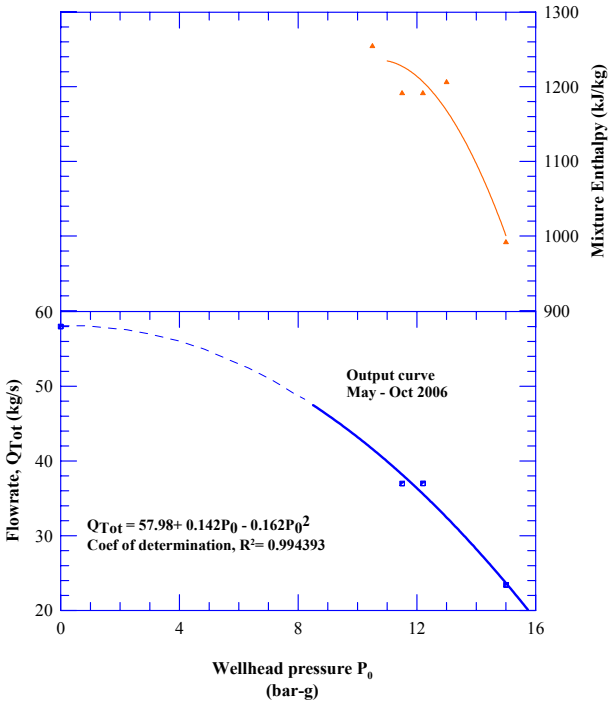

FIGURE 232: First year output curve and total enthalpy for well HE-20

The productivity index, PI, of the well was determined by comparing the dynamic pressure condition with the pressure at static conditions. The *PI* was estimated by looking at the change in pressure at the pivot point as the well was opened for discharge testing. This estimate gave *PI* = 9.1 (kg/s)/bar (i.e. 38.3/(88.9-84.7)). Results of the model used are presented in Appendix III (Table 1).

6.3 Power equivalent of discharge

The thermal power output of a well discharge can be estimated as follows:

$$MWt = Maximum\ flowrate\ (kg/s) \times [T_{inlet} - T_{outlet}] \times 0.004184$$

or

$$= Maximum\ flowrate\ (kg/s) \times [H_{inlet} - H_{outlet}] \times 0.001$$

Assuming the inlet temperature is 250°C and the outlet temperature is 0°C, for a maximum flowrate of 40 kg/s, MWt ≈ 45. However, the electrical equivalent is stated using an appropriate efficiency of conversion. For wells producing from reservoirs above 230°C and supplying a flash steam plant with a condensing turbine, efficiencies cover a range of 8-12%. Thus, HE-20 has approximately a 4.5 MWe capacity.

7. CONCLUSIONS

The warm-up, injection, and transient temperature profiles of well HE-20 revealed several feed zones but the main ones are located at about 1400, 1600 and 1800 m depths. The pressure control point was found to be located at about 1500 m depth, near the main feed zones of the well. The temperature profiles were also used to estimate the formation temperature in the well. One of the methods used (Albright) seemed to overestimate the formation temperature. The Horner method, on the other hand, made more sensible estimates. Analyses generally showed that the more reliable manner for estimating formation temperature was based on the last static temperature profile.

Temperature and pressure logs from exploration well ÖJ-1 and the two recently drilled wells, HE-20 and HE-22, were used for estimating formation temperature and the initial reservoir pressure. The permeability-thickness product (*kh*) and skin around well HE-20 were estimated to be in the range of 9 to 84 Dm and -3.0 to -0.1, respectively, whereas the storativity was on the order of 10^{-8} m/Pa s. The methods used in the analysis included semilog, type-curve matching and multirate methods, and transient pressure non-regression and derivative analysis.

The transient data used were from time periods which made it impossible to determine whether the reservoir was boundless or bounded, although prior geo-scientific studies indicate that the reservoir is a stand alone producer. Conversely, natural state models developed for the greater Hengill area are in agreement with the characteristic flow models determined from analyses of the transient data of wells in the Ölkelduháls field. Coupled with geophysical estimates of the areal size of the reservoir (20 km^2), the concepts of the model developed through analyses established that the reservoir cap rock extends to an average of 400 m depth under sea level, whereas the heat source subsides after 2000 m, thus establishing the volumetric extent of the reservoir's limits. The radius of investigation was determined to be about 3.6 km for the period of the fall-off test, though a longer test would probably enable the determination of the nature and extent of the reservoir boundaries. Interference testing was not carried out for these wells during the project. Had it been, it would have enabled the establishment of the travel time of the thermal front through pressure diffusion, re-injection points, and an initial estimate of the extent of the reservoir.

The wellbore simulator HOLA was used to simulate available dynamic temperature and pressure profiles. The enthalpy, simulated by HOLA, is reliable. The model results indicate that the productivity index for the feedzone at 1400 m is a little higher than that at the well bottom, which correlates with the pivot point location. However, the difference is not so significant, resulting in observable cycling and instability of the well's discharge. HOLA simulations indicated that lowering the reservoir pressure at the major feed zone up to 4 bar-a, in imitation of pressure decline, affects the well discharge significantly, changing the flowrate considerably. Wellbore simulation also indicated that larger diameter casing allows greater production rates, typical in geothermal fields.

Discharge analysis revealed that well HE-20 is a two-phase well. The fluid flowing into it can be liquid only or a steam/water mixture. In the former, the mixture enthalpy at the wellhead corresponds to liquid water at the formation temperature. The production test showed that HE-20 has a 4-5 MWe capacity. Analysis using the Russell-James method was found to be a good estimate for the deliverability curve of two-phase liquid feed wells with minimum data. The deliverability of steam and water from a geothermal system depends on coupling of the reservoir, inflow, and wellbore performances.

ACKNOWLEDGEMENTS

The author would like to express his gratitude to the director of UNU-GTP, Dr. Ingvar B. Fridleifsson, and the deputy director, Mr. Lúdvík S. Georgsson, together with Mrs. Gudrún Bjarnadóttir and Ms. Thórhildur Ísberg for ensuring the success of the programme.

This report exists because of relentless support from many individuals. In particular, I am indebted to the following persons in their respective capacities: my Supervisors, Mr. Benedikt S. Steingrímsson, deputy director, and Mr. Egill Júlíusson, reservoir engineer, ÍSOR - Iceland GeoSurvey; Dr. Gudni Axelsson, head of Physics Department, ÍSOR, and reservoir engineering at UNU-GTP; and Mr. Gestur Gíslason, senior geologist, Orkuveita Reykjavíkur; and all the lecturers of the different course units.

To all colleagues and friends who had a bearing on my participation and successful completion of the UNU-GTP: thumbs up.

REFERENCES

Arason, T., Björnsson, G., Axelsson, G., Bjarnason, J.Ö., and Helgason, P., 2003: *The geothermal reservoir engineering software package ICEBOX, user´s manual.* Orkustofnun, Reykjavík, report, 53 pp.

Árnason, K., 1993: *Geothermal activity in the Ölkelduhals area, resistivity soundings in* 1991 *and* 1992. Orkustofnun, Reykjavík, report OS-93037/JHD-10 (in Icelandic), 82 pp.

Árnason, K., and Magnússon, I.Th., 2001: *Geothermal activity in Hengill and at Hellisheidi. Results of resistivity measurements.* Orkustofnun, Reykjavík, report OS-2001/091 (in Icelandic), 250 pp.

Azimudin T., 1995: The Ölkelduháls geothermal field, a combined analysis of resistivity TEM soundings and down-hole data. Report 2 in: *Geothermal Training in Iceland 1995.* UNU-GTP, Iceland, 31-57.

Björnsson, A., Hersir, G.P., and Björnsson, G., 1986: The Hengill high-temperature area SW-Iceland: Regional geophysical survey. *Geothermal Resources Council, Tran., 10*, 205-210.

Björnsson, G., Arason, P., and Bödvarsson, G.S., 1993: *The wellbore simulator HOLA. Version 3.1. user's guide.* Orkustofnun, Reykjavík, 36 pp.

Bourdet, D., and Gringarten, A.C., 1980: *Log-log type curve method.* Georgia State University, website: *http://www2.gsu.edu/~geohab/courses/Geol%204008-6008/Hydro%20-%20BOURDET%20AND%20GRINGARTEN%20Log-log%20method.doc* .

Earlougher, R.C., Jr., 1977: *Advances in well test analysis*. AIME, Inc., 263 pp.

Grant, M.A., Donaldson, I.G., and Bixley, P.F., 1982: *Geothermal reservoir engineering*. Academic Press Inc., USA, 369 pp.

Gudmundsson, J.S., 1984: Discharge analysis method for two-phase geothermal wells. *Geothermal Resources Council, Trans., 8,* 295-299.

Gunnarsson, Á., Steingrímsson, B.S., Gunnlaugsson, E., Magnússon, J., and Maack, R., 1992: Nesjavellir geothermal co-generation power plant. *Geothermics, 21-4,* 559-583.

Horne, R.N., 1995: *Modern well test analysis, a computer aided approach* (2nd edition). Petroway Inc., USA, 257 pp.

Ívarsson, G., 1998: Fumaroles gas geochemistry in estimating subsurface temperatures at Hengill in south-western Iceland. *Proceedings of the 9th Symposium on Water-Rock Interaction, Balkema,* 459-462.

Kruseman, G.P., and de Ridder., N.A., 1990: *Analysis and evaluation of pumping test data* (2nd edition). International Institute for Land Reclamation and Improvement, Wageningen, Netherlands, 376 pp.

McNitt, J.R., 1982: The geothermal potential of East Africa. *Proceedings of the Regional Seminar on Geothermal Energy in Eastern and Southern Africa, Nairobi, Kenya,* 3-8.

Menzies, A.J., Gudmundsson, J.S., and Horne, R.N., 1982: Flashing flow in fractured geothermal reservoirs. *Proceedings of the 8th Workshop of Geothermal Reservoir Engineering*, *Stanford University, Ca,* 143-147.

Mortensen, A.K., Gudmundsson, Á., Egilsson, Th., Bliscke, A., Jónsson, S.S., Gautason, B., Ásmundsson, R.K., Danielsen, P.E., Hjartarson, A., Sigurdsson, G., Björnsson, G., Sigurdsson, Ó., and Thorgrímsson, A.K., 2006: *Ölkelduháls – well HE-20. 3rd part: Drilling of 8½" production part from 706 m to 2002 m depth.* ÍSOR, Reykjavík, report ÍSOR-2006/034 (in Icelandic), 178 pp.

Natukunda J.F., 2005. Geothermal mapping in eastern Ölkelduháls field, Hengill area, SW-Iceland. Report 14 in: *Geothermal Training in Iceland 2005*. UNU-GTP, Iceland, 247-264.

Pruess, K. and Finsterle, S., 1996: *Design and analysis of a well test for determining two-phase hydraulic properties*. Lawrence Berkeley National Laboratory, Earth Sciences Division, University of California, Berkeley, CA, 38 pp.

Saemundsson, K., 1979: Outline of the geology of Iceland. *Jökull*, *29*, 7-28.

Saemundson, K., 1995: *Geological map of the Hengill area, 1:25,000.* Orkustofnun, Reykjavík.

Saemundsson, K., Snorrason, S.P., and Fridleifsson, G.Ó., 1990: *Geological map of the southern Hengill area, between Hengladalir and Krossfjöll*. Orkustofnun, Reykjavik, report OS-90008/JHD-02B, 15 pp.

Stefánsson, V., and Steingrímsson, B.S., 1990: *Geothermal logging I, an introduction to techniques and interpretation* (3rd edition). Orkustofnun, Reykjavík, report OS-80017/JHD-09, 117 pp.

Steingrímsson, B., Tulinius, H., Franzson, H., Sigurdsson, Ó., Gunnlaugsson, E., Gíslason, G., 1997: *Ölkelduháls, well ÖJ-1. Drilling, exploration and production characteristics. Final report* (in Icelandic). Orkustofnun, Reykjavík, report OS-97019, 190 pp.

APPENDIX I: General information of wells drilled in the Ölkelduháls geothermal field

Well **OS.STADUR Id** **Observations**		**ÖJ-1** **95101** **V, E**	**HE-20** **95120** **D, P**	**HE-22** **95122** **D, P**
Drilling finished		1995-Jan-22	2005-Dec-11	2006-Jul-19
Location	**Latitude** **Longitude**	396972.7 390146.2	397084.4 390742.5	397420 389945
Elevation (m a.s.l.) **Measured depth (m)**		360.93 1035	350 2002	374 2104
Casing (m)	**18 5/8"** **13 3/8"** **9 5/8"**	79 301 777	99.5 285.0 693.0	311 1062,5
Slotted liner (m)	**18 5/8"** **13 3/8"** **9 5/8"** **7"**	 734-1013	 650-1980	 1000-2084

D-Directional well; E: Exploration well; P-Production well; V-Vertical well;

APPENDIX II: Well test calculation

A. Theis solution (semilog analysis)

Table 1 shows well test data from HE-20 used in calculations

Transmissivity:

$$T = \frac{kh}{\mu} = \frac{2.303(0.05 - 0.013)}{4\pi \times 351666.1} = 1.93 \times 10^{-8}\ m^3 Pa \ \ and \ \ kh = T\mu, \ or \ \ 25 \times 10^{-12}\ m^3\ (25\ Dm)$$

Storativity:

$$c_t he^{-2s} = 2.246 \times 1.93 \times 10^{-8} \left(\frac{3600}{(0.1222375)^2} \right) \times 10^{\frac{-738483.4}{351666.1}} \ = \ 8.3038 \times 10^{-5}\ m/Pa.s$$

Equation 8 holds for $t > 100\frac{\mu c_t r^2}{4k}$. As a consistency check, the dimensionless time at which the reservoir response begins can be estimated from:

$$t = 100 \times \frac{0.0013 \times 4.37647 \times 10^{-5} \times (0.1222375)^2}{4 \times 2.5 \times 10^{-11}} = 847.85\ \text{s}$$

However, the data used is between 1100 and 4161 seconds so the semilog straight used line is a good approximation.

Equation 8 is the equation most used in well test analysis and describes pressure draw-down at a distance r at time t when producing/injecting at constant rate q (m^3/s) in a reservoir model. In this solution $\bar{q} = \Delta q$.

Wellbore storage:
The wellbore storage coefficient C, for a free surface, is estimated as 4.782×10^{-6} Pa^{-1}, using Equation 16.

TABLE 1: Well test data from HE-20

Flow periods (s)	
0-40	Wellbore storage
40-1100	Transition zone
>1100	Infinite acting
Pertinent data	
T_1	7800 s
M	0.0013 kg/ms
Φ	14%
r_w	0.1222375 m
Slope, m	351666.1 Pa/log cycle
Q_1	-50 m^3/s
Q_2	-13 m^3/s
ΔP(at t = 1 hr)	738483.4 Pa
P	999.7 kg/m^3
G	9.82 m/s^2

B. Theis type curve matching

Match point data:

$(P_D)_M = 6.2 \times 10^{-2}$.; $(t_D/r_D^2)_M = 10^3$

$(\Delta P)_M = 10^4$; $(\Delta t)_M = 10^3$

By substituting the ordinate match point values obtained for an infinite acting system, the transmissivity, T, is estimated as:

$$T = \frac{kh}{\mu} = \frac{\bar{q}}{2\pi}\left(\frac{P_D}{\Delta P}\right)_M = \frac{(5.0 - 1.3) \times 10^{-2}}{2\pi}\left(\frac{6.2 \times 10^{-2}}{10^4}\right)_M = 3.651 \times 10^{-8}\ \text{m}^3/\text{Pa.s}$$

Permeability thickness is then estimated as $kh = T\mu$ *or* 4.7463×10^{-11} m^3 *(or 47.5 Dm).*

Similarly using the definition on the abscissa of the type curve, storativity can subsequently be calculated from:

$$S = \frac{kh}{\mu r_w^2}\left(\frac{\Delta t}{t_D}\right)_M = \frac{3.651\times10^{-8}}{(0.1222375)^2}\left(\frac{10^3}{10^3}\right)_M = 2.4434\times10^{-6} \text{ m/Pa.s.}$$

Skin:
Using the storativity values of the semilog, 8.304×10^{-5} m/Pa.s and Theis type curve analysis 2.44345×10^{-6} m/Pa.s, we estimate skin as -1.7629, thus:

$$\frac{c_t h e^{-2s}\ (semilog)}{c_t h\ (Theis\ \ type\ \ curve)} = e^{-2s} \quad and \quad from \quad \frac{8.30377\ \times10^{-5}}{2.44345\ \times10^{-6}}, \quad s = -\frac{1}{2} ln\ 33.984\ \ = -1.763$$

C. Type curves and derivative analysis

Wellbore storage affects the early data which, in a double porosity medium, represents the most permeable medium (i.e., fractures); thus, the first semilog straight line predicted by the Warren and Root model, seldom appears in practical cases. To avoid this masking effect in multilayered reservoirs, a downhole shut-in tool can be used. For fractured rocks, however, the total storage effect includes the wellbore storage and storage of fractures intersecting the well, which is one or two orders of magnitude greater than the wellbore storage. The discussion below is mainly based on Bourdet and Gringarten (1980); original references used there can be found in their presentation.

Bourdet and Gringarten (1980) presented a log-log type curve method for analyzing wells with wellbore storage and skin in an infinite double porosity reservoir. In addition to permeability, skin, wellbore storage constant, and length of fractures intersecting the well, the method yields, even in the absence of both early and late time data, quantitative information on the volume of fractures and the size of porous blocks.

The wellbore storage and skin solution of Mavor and Cinco was used to find parameters which allow the construction of type-curves that yield all the reservoir parameters, even when they cannot be obtained on semilog analysis.

It was shown that the double porosity behaviour is controlled by several independent variables, such as p_D, t_D/C_D. C_De^{2s}, ω, and λe^{-2s}, where t_D/C_D is the dimensionless time defined by:

$$t_D/C_D = 2\pi kh\Delta t/\mu C$$

where k = Reservoir permeability;
C = Wellbore storage constant (coefficient);
s = Infinitesimal skin; and
ω & λ = The Warren and Root double porosity parameters defined above.

Here, $\lambda < 1.78$, which represents the local effect of the double porosity behaviour around a pumping well. The radius of influence depends on λ. Beyond this value ($\lambda > 1.78$), the drawdown behaviour is that of the homogeneous, isotropic total reservoir of fractures and matrix (Kruseman and de Ridder, 1990). C_D is the dimensionless wellbore storage constant and is equal to:

$$C_D = (C_D)_f = C \Big/ 2\pi\phi_f v_f (ct)_f h r_w^2$$

where ϕ_f = Fracture porosity;
v_f = The ratio of total volume of fracture to bulk volume;
h = Total reservoir thickness;
r_w = Radius of the well;
$(ct)_f$ = Total compressibility of fracture.

The equation in late times involves both the fracture and matrix characteristics:

$$C_D = (C_D)_{f+m} = C \Big/ 2\pi\left[\phi_f v_f (ct)_f + \phi_m v_m (ct)_m\right] h r_w^2$$

Two equations (not shown in this report) were derived for the dimensionless pressure p_D for both early and late times, such that: $p_D = f(t_D/C_D, C_D e^{2s}, \omega, \lambda e^{-2s})$. The two equations are identical for early and late times except for the value of C_D. Both represent the pressure behaviour of a well with a wellbore storage and skin in a homogeneous reservoir, corresponding to two different curves on the wellbore storage and skin type-curves on a pD versus t_D/C_D plot.

Bourdet and Gringarten showed that the problem of a well with wellbore storage and skin in a double porosity reservoir is broken into two parts: First, the problem of a well with wellbore storage and skin in a homogeneous medium with type curves, and then the effect of the double porosity medium, represented by the λe^{-2s} curves. The superposition of the two type curves provides the drawdown type curve for a well with wellbore storage and skin in a double porosity reservoir.

When a well with storage and skin is pumped at a constant rate in a double porosity reservoir, the well pressure data follows this path: At early times, when production comes from the most permeable medium, e.g. fractures, the pressure data follow one of the homogeneous $C_D e^{2S}$ curves, with $C_D = (C_D)_f$. Then the drawdown response follows the Theis equation: $s = q/4\pi T\ W(u)$, where $u = (s_f = \beta s_m) r^2/4T_f t$ and f and m refer to fracture and matrix, respectively, β is a factor which is equal to zero at early times, and 1/3 for orthogonal system of fractures, and equal to 1 for layered reservoirs (Kruseman and de Ridder, 1990).

In intermediate times, when blocks start to contribute to fractures, the pressure leaves the $C_D e^{2S}$ curve, and being solely a function of λ, it follows a transitional λe^{-2S} curve. The drawdown response in the intermediate time is (Kruseman and de Ridder, 1990): $s = q/2\pi T_f K_o(\sqrt{\lambda})$, where $K_o(x)$ is the modified Bessel function of the second kind and of the zero order for $\lambda < 0.01$. Then the equation becomes:

$$s = 2.303 q/2\pi T_f \log 1.26/\lambda.$$

The pressure response in late times again follows a homogeneous $C_D e^{2S}$ curve, below the first $C_D e^{2S}$ curve, when production starts to come from the entire matrix and fracture system, i.e., when $C_D = (C_D)_{f+m}$, which corresponds to homogeneous behaviour of the total reservoir. When $(\varphi v c_t)_f$ is very small compared to $(\varphi v c_t)_{f+m}$, the fracture $C_D e^{2S}$ curve coincides with the transitional λe^{-2S} curve from the very beginning before merging into a total system $(C_D e^{2S})_{f+m}$ curve.

Matching the pressure data with the type curves yields the following:

a) $k_f h$ from the pressure match;
b) C from the time match;
c) s from the $C_D e^{2S}$ curve for which $\varphi v c_t$ is available;
d) λ from λe^{-2S} curve; and
e) ω from ratio of the last $C_D e^{2S}$ value to the first $C_D e^{2S}$ value: $\omega = (C_D e^{2S})_{f+m} / (C_D e^{2S})f$.

APPENDIX III: Observed and calculated data

TABLE 1: Model results from simulation of wellbore conditions of well HE-20

HOLA Wellbore simulator- model results
Well HE-20

Wellhead	pressure (bar-a)	: 11.2
Wellhead	temperature (°C)	: 184.87
Wellhead	dryness (%)	: 13.75
Wellhead	enthalpy (kJ/kg)	: 1059
Wellhead	total flow (kg/s)	: 38.3

Depth (m)	Press (bar-a)	Temp (°C)	Dryness (%)	Hw (kJ/kg)	Hs (kJ/kg)	Ht (kJ/kg)	Vw (m/s)	Vs (m/s)	Dw (kg/m3)	Ds (kg/m3)	Rad (mm)	Reg
0	11.2	184.9	13.7	785	2780	1059	2.48	11.63	881.7	5.7	173	Sl
230	15.9	201	10.8	857	2792	1065	1.97	6.94	863.5	8	173	Sl
460	22.1	217.5	7.4	932	2799	1071	1.51	3.86	843.5	11.1	173	Sl
690	31.1	235.8	3.3	1018	2802	1076	1	1.65	819.5	15.5	173	Bu
700	31.6	236.7	3.1	1022	2802	1076	1.96	3.14	818.3	15.8	122	Sl
710	32.1	237.6	2.9	1026	2802	1077	1.9	2.96	817	16.1	122	Sl
720	32.6	238.5	2.6	1030	2802	1077	1.84	2.79	815.7	16.3	122	Sl
730	33.1	239.4	2.4	1035	2802	1077	1.78	2.61	814.4	16.6	122	Sl
740	33.7	240.4	2.2	1039	2802	1077	1.72	2.44	813.1	16.9	122	Sl
750	34.3	241.3	1.9	1044	2802	1078	1.65	2.26	811.7	17.2	122	Sl
760	34.9	242.3	1.7	1049	2802	1078	1.58	2.09	810.3	17.5	122	Sl
770	35.5	243.3	1.4	1054	2802	1078	1.5	1.91	808.9	17.8	122	Sl
780	36.1	244.4	1.1	1059	2802	1078	1.42	1.74	807.4	18.1	122	Bu
790	36.8	245.4	0.9	1064	2802	1079	1.33	1.56	805.9	18.5	122	Bu
800	37.5	246.5	0.6	1069	2801	1079	1.23	1.37	804.3	18.8	122	Bu
810	38.2	247.7	0.3	1074	2801	1079	1.12	1.19	802.6	19.2	122	Bu
820	39	248.7	0	1079	2802	1079	1.02	4.31	801.1	14	122	1p
830	39.8	248.7	0	1080	2802	1080	1.02	4.19	801.2	14.2	122	1p
840	40.6	248.8	0	1080	2802	1080	1.02	4.06	801.2	14.4	122	1p
850	41.4	248.8	0	1080	2802	1080	1.02	3.94	801.2	14.6	122	1p
860	42.2	248.9	0	1080	2802	1080	1.02	3.82	801.2	14.7	122	1p
870	43	248.9	0	1081	2802	1081	1.02	3.69	801.2	14.9	122	1p
880	43.7	249	0	1081	2802	1081	1.02	3.57	801.2	15.2	122	1p
890	44.5	249	0	1081	2802	1081	1.02	3.44	801.3	15.4	122	1p
900	45.3	249.1	0	1081	2802	1081	1.02	3.32	801.3	15.6	122	1p
910	46.1	249.1	0	1081	2802	1081	1.02	3.19	801.3	15.8	122	1p
920	46.9	249.2	0	1082	2802	1082	1.02	3.06	801.3	16.1	122	1p
930	47.7	249.2	0	1082	2802	1082	1.02	2.93	801.3	16.3	122	1p
940	48.5	249.3	0	1082	2802	1082	1.02	2.8	801.3	16.6	122	1p
950	49.3	249.3	0	1082	2802	1082	1.02	2.66	801.4	16.9	122	1p
960	50	249.4	0	1083	2802	1083	1.02	2.52	801.4	17.2	122	1p
970	50.8	249.4	0	1083	2802	1083	1.02	2.38	801.4	17.5	122	1p
980	51.6	249.4	0	1083	2802	1083	1.02	2.23	801.4	17.9	122	1p
990	52.4	249.5	0	1083	2802	1083	1.02	1.61	801.4	18.2	122	1p
1000	53.2	249.5	0	1084	2801	1084	1.02	1.66	801.5	18.5	122	1p
1010	54	249.6	0	1084	2801	1084	1.02	1.53	801.5	18.9	122	1p
1020	54.8	249.6	0	1084	2801	1084	1.02	1.39	801.5	19.3	122	1p
1030	55.6	249.7	0	1084	2801	1084	1.02	1.25	801.5	19.7	122	1p
1040	56.4	249.7	0	1084	0	1084	1.02	0	801.5	0	122	1p
1050	57.1	249.8	0	1085	0	1085	1.02	0	801.6	0	122	1p
1060	57.9	249.8	0	1085	0	1085	1.02	0	801.6	0	122	1p
1070	58.7	249.9	0	1085	0	1085	1.02	0	801.6	0	122	1p
1080	59.5	249.9	0	1085	0	1085	1.02	0	801.6	0	122	1p
1090	60.3	250	0	1086	0	1086	1.02	0	801.7	0	122	1p
1100	61.1	250	0	1086	0	1086	1.02	0	801.7	0	122	1p
1110	61.9	250	0	1086	0	1086	1.02	0	801.7	0	122	1p
1120	62.7	250.1	0	1086	0	1086	1.02	0	801.7	0	122	1p
1130	63.5	250.1	0	1086	0	1086	1.02	0	801.7	0	122	1p
1140	64.2	250.2	0	1087	0	1087	1.02	0	801.8	0	122	1p
1150	65	250.2	0	1087	0	1087	1.02	0	801.8	0	122	1p
1160	65.8	250.3	0	1087	0	1087	1.02	0	801.8	0	122	1p
1170	66.6	250.3	0	1087	0	1087	1.02	0	801.8	0	122	1p
1180	67.4	250.3	0	1087	0	1087	1.02	0	801.9	0	122	1p
1190	68.2	250.4	0	1088	0	1088	1.02	0	801.9	0	122	1p
1200	69	250.4	0	1088	0	1088	1.02	0	801.9	0	122	1p
1210	69.8	250.5	0	1088	0	1088	1.02	0	801.9	0	122	1p
1220	70.6	250.5	0	1088	0	1088	1.02	0	802	0	122	1p
1230	71.3	250.6	0	1088	0	1088	1.02	0	802	0	122	1p
1240	72.1	250.6	0	1089	0	1089	1.02	0	802	0	122	1p
1250	72.9	250.6	0	1089	0	1089	1.02	0	802	0	122	1p
1260	73.7	250.7	0	1089	0	1089	1.02	0	802.1	0	122	1p
1270	74.5	250.7	0	1089	0	1089	1.02	0	802.1	0	122	1p
1280	75.3	250.8	0	1089	0	1089	1.02	0	802.1	0	122	1p
1290	76.1	250.8	0	1090	0	1090	1.02	0	802.2	0	122	1p
1300	76.9	250.8	0	1090	0	1090	1.02	0	802.2	0	122	1p
1310	77.7	250.9	0	1090	0	1090	1.02	0	802.2	0	122	1p
1320	78.5	250.9	0	1090	0	1090	1.02	0	802.2	0	122	1p
1330	79.2	251	0	1090	0	1090	1.02	0	802.3	0	122	1p
1340	80	251	0	1091	0	1091	1.02	0	802.3	0	122	1p
1350	80.8	251	0	1091	0	1091	1.02	0	802.3	0	122	1p
1360	81.6	251.1	0	1091	0	1091	1.02	0	802.4	0	122	1p
1370	82.4	251.1	0	1091	0	1091	1.02	0	802.4	0	122	1p
1380	83.2	251.2	0	1091	0	1091	1.02	0	802.4	0	122	1p
1390	84	251.2	0	1092	0	1092	1.02	0	802.4	0	122	1p
1400	84.8	251.2	0	1092	0	1092	1.02	0	802.5	0	122	1p
1400	84.8	256.2	0	1116	0	1116	0.49	0	794.9	0	122	1p
.....	.....	.....	.....	.....	.....	.....	.....	.....	.....	.....	.....	1p
.....	.....	.....	.....	.....	.....	.....	.....	.....	.....	.....	.....	1p
1910	124.6	258.8	0	1128	0	1128	0.49	0	795.5	0	122	1p
1920	125.4	258.8	0	1128	0	1128	0.49	0	795.6	0	122	1p
1930	126.1	258.8	0	1128	0	1128	0.49	0	795.6	0	122	1p
1940	126.9	258.9	0	1129	0	1129	0.49	0	795.6	0	122	1p
1950	127.7	258.9	0	1129	0	1129	0.49	0	795.7	0	122	1p
1960	128.5	259	0	1129	0	1129	0.49	0	795.7	0	122	1p
1970	129.3	259	0	1129	0	1129	0.49	0	795.7	0	122	1p
1980	130	259	0	1129	0	1129	0.49	0	795.8	0	122	1p
1990	130.8	259.1	0	1130	0	1130	0.49	0	795.8	0	122	1p
2000	131.6	259.1	0	1130	0	1130	0.49	0	795.8	0	122	1p

TABLE 2: Fall-off test (5) data used for the two step test, semilog and type curve methods

Time, t [sec]	Pressure [bar-a]	Δt [sec]	Pressure P_{wf}[Pa]	$\log\left(\frac{t_1+\Delta t}{\Delta t}\right)$	$\log \Delta t$	$\log\left(\frac{t_1+\Delta t}{\Delta t}\right)+\frac{q_2}{q_1}\log \Delta t$	ΔP Pa
0	34.8	0	3480000	STEP START			
5	34.51	5	3451000	3.1934029	0.69897	3.375135104	29000
16	34.07	16	3407000	2.68886457	1.20412	3.001935764	73000
27	34.17	27	3417000	2.46223157	1.431364	2.834386148	63000
32	33.85	32	3385000	2.3887227	1.50515	2.780061695	95000
61	33.42	61	3342000	2.11014796	1.78533	2.574333718	138000
72	33.09	72	3309000	2.03875259	1.857332	2.521659038	171000
77	33.32	77	3332000	2.00987012	1.886491	2.500357709	148000
82	33.09	82	3309000	1.98282258	1.913814	2.48041418	171000
87	32.79	87	3279000	1.95739259	1.939519	2.461667594	201000
110	32.25	110	3225000	1.8567838	2.041393	2.387545896	255000
121	32.09	121	3209000	1.81599464	2.082785	2.357518839	271000
138	31.6	138	3160000	1.75983201	2.139879	2.316200571	320000
155	31.29	155	3129000	1.71030849	2.190332	2.279794727	351000
3013	27.59	3013	2759000	0.55494707	3.478999	1.459486846	721000
-	-	-	-	-	-	-	-
-	-	-	-	-	-	-	-
3030	27.28	3030	2728000	0.55318583	3.481443	1.458360912	752000
3035	27.76	3035	2776000	0.55267022	3.482159	1.458031481	704000
3040	27.48	3040	2748000	0.5521557	3.482874	1.45770283	732000
3051	27.73	3051	2773000	0.55102756	3.484442	1.45698253	707000
3068	27.35	3068	2735000	0.54929427	3.486855	1.455876667	745000
3073	27.63	3073	2763000	0.54878683	3.487563	1.455553093	717000
3131	27.31	3131	2731000	0.54297683	3.495683	1.451854424	749000
3136	27.3	3136	2730000	0.54248245	3.496376	1.451540222	750000
3141	27.55	3141	2755000	0.54198908	3.497068	1.451226745	725000
3152	27.44	3152	2744000	0.54090723	3.498586	1.450539641	736000
3193	27.5	3193	2750000	0.53691731	3.504199	1.448009028	730000
3216	27.77	3216	2777000	0.53470789	3.507316	1.446610058	703000
3257	27.38	3257	2738000	0.53081955	3.512818	1.444152168	742000
3315	27.64	3315	2764000	0.52542593	3.520484	1.440751653	716000
3350	27.41	3350	2741000	0.52223006	3.525045	1.43874171	739000
3361	27.61	3361	2761000	0.5212346	3.526469	1.438116409	719000
3378	27.36	3378	2736000	0.51970446	3.52866	1.437155968	744000
3389	27.81	3389	2781000	0.51871971	3.530072	1.436538313	699000
3394	27.48	3394	2748000	0.51827346	3.530712	1.436258542	732000
3435	27.66	3435	2766000	0.51464634	3.535927	1.433987288	714000
3493	27.37	3493	2737000	0.50961074	3.543199	1.430842375	743000
3557	27.53	3557	2753000	0.50417976	3.551084	1.427461566	727000
3568	27.37	3568	2737000	0.50325922	3.552425	1.426889679	743000
3614	27.58	3614	2758000	0.49944972	3.557988	1.424526639	722000
3678	27.53	3678	2753000	0.4942545	3.565612	1.421313544	727000
3736	27.35	3736	2735000	0.48964838	3.572407	1.418474165	745000
3747	27.61	3747	2761000	0.48878547	3.573684	1.417943233	719000
3758	27.41	3758	2741000	0.48792591	3.574957	1.417414676	739000
3769	27.66	3769	2766000	0.48706968	3.576226	1.416888479	714000
3798	27.44	3798	2744000	0.48482814	3.579555	1.415512434	736000
3856	27.35	3856	2735000	0.48041251	3.586137	1.41280814	745000
3914	27.44	3914	2744000	0.4760844	3.592621	1.410165812	736000
3978	27.37	3978	2737000	0.47140677	3.599665	1.407319614	743000
3989	27.61	3989	2761000	0.47061293	3.600864	1.406837581	719000
4035	27.51	4035	2751000	0.46732472	3.605844	1.404844043	729000
4093	27.46	4093	2746000	0.46324967	3.612042	1.402380528	734000
4122	27.23	4122	2723000	0.46124113	3.615108	1.401169207	757000
4127	27.51	4127	2751000	0.46089675	3.615634	1.400961712	729000
4156	27.23	4156	2723000	0.45891037	3.618676	1.399766008	757000
4161	27.51	4161	2751000	0.45856977	3.619198	1.399561181	729000

TABLE 3: Falloff test (5) data from well HE-20 used for the derivative plot and analysis

Time, t [sec]	Pressure [bar-a]	Δt [sec]	Δp [Pa]	t.dp/dt [Pa]	p calc [Pa]	t.dp/dt calc [Pa]	P (Pa)
0	34.8	0	0	STEP START			
5	34.51	5	29000	22812.50	13264.94	12836.26977	3451000
16	34.07	16	73000	24727.27	41076.06	39320.85817	3407000
27	34.17	27	63000	37125.00	67331.12	63662.28652	3417000
32	33.85	32	95000	70588.24	78801.86	68615.59104	3385000
61	33.42	61	138000	115900.00	140235.19	126065.4514	3342000
72	33.09	72	171000	45000.00	161467.73	137423.7667	3309000
77	33.32	77	148000	0.00	170773.80	141714.0572	3332000
82	33.09	82	171000	434600.00	179872.16	147553.7884	3309000
2834	27.64	2834	716000	114505.05	747457.49	115087.7482	2764000
2898	27.46	2898	734000	716709.68	750040.37	116365.7511	2746000
-	-	-	-	-	-	-	-
-	-	-	-	-	-	-	-
2927	27.41	2927	739000	-857913.79	751191.80	115633.418	2741000
2956	27.63	2956	717000	-2191517.24	752331.71	115614.6558	2763000
2985	27.84	2985	696000	1377692.31	753460.29	115711.1997	2784000
3008	27.39	3008	741000	2685714.29	754347.45	115926.2994	2739000
3013	27.59	3013	721000	1506500.00	754539.39	115332.4757	2759000
3030	27.28	3030	752000	-2341363.64	755189.57	115787.0099	2728000
3035	27.76	3035	704000	-6070000.00	755380.09	115547.3131	2776000
3040	27.48	3040	732000	570000.00	755570.28	115426.114	2748000
3051	27.73	3051	707000	1416535.71	755987.59	115416.527	2773000
3068	27.35	3068	745000	1394545.45	756629.50	115748.2082	2735000
3073	27.63	3073	717000	195111.11	756817.60	114498.5324	2763000
3131	27.31	3131	749000	1640047.62	758976.85	116466.1802	2731000
3136	27.3	3136	750000	-7526400.00	759161.06	115440.991	2730000
3141	27.55	3141	725000	-2748375.00	759344.96	115321.4249	2755000
3152	27.44	3152	736000	303076.92	759748.50	114859.128	2744000
3193	27.5	3193	730000	-1646390.62	761239.85	115711.6647	2750000
3216	27.77	3216	703000	603000.00	762067.80	115009.4147	2777000
3257	27.38	3257	742000	427686.87	763528.59	114979.3618	2738000
3315	27.64	3315	716000	-106935.48	765562.72	115623.6133	2764000
3350	27.41	3350	739000	218478.26	766772.33	115578.2195	2741000
3361	27.61	3361	719000	600178.57	767149.77	115019.4799	2761000
3378	27.36	3378	744000	-2412857.14	767730.54	115206.8845	2736000
3389	27.81	3389	699000	-2541750.00	768104.71	115188.248	2781000
3394	27.48	3394	732000	1106739.13	768274.36	114438.2256	2748000
3435	27.66	3435	714000	381666.67	769655.73	114714.6094	2766000
3493	27.37	3493	743000	372204.92	771580.55	114813.0462	2737000
3557	27.53	3557	727000	0.00	773665.80	115705.2165	2753000
3568	27.37	3568	743000	-312982.46	774020.21	114181.4711	2737000
3614	27.58	3614	722000	-525672.73	775489.89	114393.621	2758000
3678	27.53	3678	727000	693393.44	777502.04	114675.7763	2753000
3736	27.35	3736	745000	-433159.42	779293.71	115227.844	2735000
3747	27.61	3747	719000	-1021909.09	779630.17	114433.2299	2761000
3758	27.41	3758	739000	-854090.91	779965.59	114411.809	2741000
3769	27.66	3769	714000	-282675.00	780299.96	114101.034	2766000
3798	27.44	3798	736000	1353310.34	781176.53	113874.9654	2744000
3856	27.35	3856	745000	0.00	782908.47	114227.3839	2735000
3914	27.44	3914	736000	-64163.93	784612.83	114018.8318	2744000
3978	27.37	3978	743000	-901680.00	786462.45	114795.5118	2737000
3989	27.61	3989	719000	-979754.39	786777.15	113420.6604	2761000
4035	27.51	4035	729000	581971.15	788083.16	113684.045	2751000
4093	27.46	4093	734000	1317287.36	789707.30	114179.5095	2746000
4122	27.23	4122	757000	-606176.47	790510.13	114039.2031	2723000
4127	27.51	4127	729000	0.00	790647.94	113318.8724	2751000
4156	27.23	4156	757000	0.00	791443.70	113967.2984	2723000
4161	27.51	4161	729000	757910.73	791580.30		2751000